NASA TECHNICAL NOTE

NASA TN D-8203

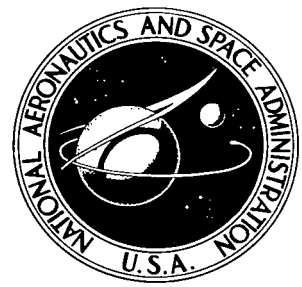

NASA TN D-8203

SHOCK INTERFERENCE HEAT TRANSFER TO TANK CONFIGURATIONS MATED TO A STRAIGHT-WING SPACE SHUTTLE ORBITER AT MACH NUMBER 10.3

Davis H. Crawford

Langley Research Center
Hampton, Va. 23665

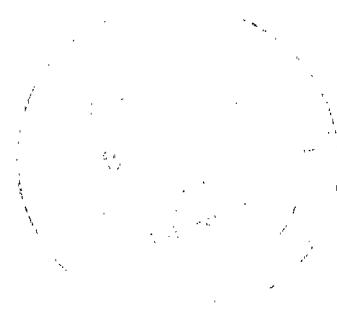

NATIONAL AERONAUTICS AND SPACE ADMINISTRATION • WASHINGTON, D. C. • APRIL 1976

1. Report No.	2. Government Accession No.	3. Recipient's Catalog No.
NASA TN D-8203		

4. Title and Subtitle	5. Report Date
SHOCK INTERFERENCE HEAT TRANSFER TO TANK CONFIGURATIONS MATED TO A STRAIGHT-WING SPACE SHUTTLE ORBITER AT MACH NUMBER 10.3	April 1976
	6. Performing Organization Code
7. Author(s)	8. Performing Organization Report No.
Davis H. Crawford	L-10441
	10. Work Unit No.
9. Performing Organization Name and Address	506-26-10-07
NASA Langley Research Center Hampton, Va. 23665	11. Contract or Grant No.
	13. Type of Report and Period Covered
12. Sponsoring Agency Name and Address	Technical Note
National Aeronautics and Space Administration Washington, D.C. 20546	14. Sponsoring Agency Code

15. Supplementary Notes

16. Abstract

Heat transfer has been measured on a space shuttle-tank configuration with no mated orbiter in place and with the orbiter in 10 different mated positions. The orbiter-tank combination was tested at angles of attack of 0^{o} and 5^{o}, at a Mach number of 10.3, and at a free-stream Reynolds number of 10^{6} based on the length of the tank. Comparison of interference heat transfer with no-interference heat transfer shows that shock interference can increase the heat transfer to the tank by two orders of magnitude along the ray adjacent to the orbiter and can cause high temperature gradients along the tank skin. The relative axial location of the two mated vehicles determined the location of the sharp peaks of extreme heating as well as their magnitude. The other control variables (the angle of attack, the gap, and the cross-section shape) had significant effects that were not as consistent or as extreme.

17. Key Words (Suggested by Author(s))	18. Distribution Statement
Shock interference heating Shock—boundary-layer interaction Shock interactions Space shuttle	Unclassified – Unlimited Subject Category 34

19. Security Classif. (of this report)	20. Security Classif. (of this page)	21. No. of Pages	22. Price*
Unclassified	Unclassified	48	$3.75

*For sale by the National Technical Information Service, Springfield, Virginia 22161

SHOCK INTERFERENCE HEAT TRANSFER TO TANK CONFIGURATIONS MATED TO A STRAIGHT-WING SPACE SHUTTLE ORBITER AT MACH NUMBER 10.3

Davis H. Crawford
Langley Research Center

SUMMARY

The aerothermodynamic effect of shock interference on an external tank mated with an early straight-wing shuttle orbiter has been studied at a Mach number of 10.3 and at a free-stream Reynolds number of 10^6 based on the tank length. Local heat transfer has been determined from transient thin-skin temperature measurements. The investigation was a parametric study of shock interference heat transfer for two mated bodies with the relative axial location, the angle of attack, the gap, and the cross-section shape (cylindrical or flat) exposed to the impinging shock as control variables.

Comparison of interference heat transfer with no-interference heat transfer shows that shock interference can increase the heat transfer to the tank by two orders of magnitude along the ray adjacent to the orbiter and can cause high temperature gradients along the tank skin. The relative axial location of the two mated vehicles determined the location of the sharp peaks of extreme heating as well as their magnitude. The other control variables (the angle of attack, the gap, and the cross-section shape) had significant effects that were not as consistent or as extreme.

INTRODUCTION

Previous aerodynamic configurations have often featured the use of bodies in close proximity. In hypersonic flight, such bodies may suffer localized thermal damage and mechanical strain problems because of shock interference heating. Nevertheless, recent launch vehicles have such bodies,[1] and the present space shuttle features mated bodies at take-off.

Shock interference flow can form many complicated patterns (refs. 1, 2, and 3). These have been classified in six general types (ref. 1). The heat transfer resulting from shock interference is strongly dependent on the type of shock interference pattern

[1]The Titan has strap-on motors which separate after reaching a Mach number greater than 5 and an altitude greater than 30 000 m.

formed, and the positions and magnitudes of heating are a direct function of the shape of the interacting shocks. A better understanding of shock interference patterns and their relation to aerodynamic heating will aid in the design of mated bodies shaped to minimize the total heating, to hold the heat transfer peaks to within reasonable limits, and to allow the design of heat shielding with a minimum weight penalty.

The experimental investigation reported in the present paper is a parametric study of two-body interference heating intended to augment the empirical understanding of the effect of shock interference aerothermal heating. Confirmation of earlier measurements (ref. 4) concerning maximum heat transfer multiplication factors and of the general shape of heat transfer in an interference region was also anticipated. The tank construction featured a cylindrical cross-section shape over 240° of its periphery and a plane face diametrically opposed to this cylindrical surface. Thus, by rotating the tank, a comparison of interference heat transfer on the cylindrical side with that on the flat side was obtained. Axial and radial positions of the orbiter with respect to the tank were adjustable for study of the effects of different longitudinal locations and gaps upon interference heat transfer. The orbiter-tank combination was tested at two attitudes to determine the effect of a change in angle of attack. By using these control variables, different effects of shock interference upon heat transfer were observed.

This series of tests was performed in the Langley continuous-flow hypersonic tunnel at a Mach number of 10.3 and a Reynolds number of 10^6 based on tank length. The combination was tested at 0° and 5° angle of attack. The orbiter was positioned at three axial locations alongside the tank: the nose of the orbiter even with the nose of the tank, 17 percent behind the nose of the tank, and 34 percent behind the nose of the tank. The three gap dimensions used were 0, 0.17 percent of the tank length, and 0.34 percent of the tank length.

SYMBOLS

c	wing root chord
c_p	specific heat of model skin
h	heat transfer coefficient
h_{ref}	reference stagnation point heat transfer coefficient
L	length of tank
l	axial distance from nose of tank to station on surface of tank

M	Mach number
M_∞	Mach number upstream of any part of model shock pattern
R	radius of tank
T_{aw}	adiabatic wall temperature
T_w	wall temperature
t	thickness of model skin
X,Y,Z	axis of orbiter with origin at nose (see fig. 2)
x,y,z	coordinates along X-, Y-, and Z-axis
α	angle of attack of tank
Δ	axial distance from orbiter nose to tank nose (see fig. 4)
δ	minimum gap spacing between mated vehicles
ρ_m	density of model skin
τ	time
ϕ	peripheral angle (see fig. 1)

APPARATUS AND TESTS

Models

The tank model shown in figure 1 was constructed of inconel sheet. The cross-section shape, which was constant over the downstream 60 percent of the tank, was circular over 240^o of its circumference, with part of a regular hexagon with rounded corners circumscribed over the remaining 120^o of the circumference. The rounded corners of 0.90-cm radius retained this radius as the tank cross section decreased in size toward the nose until a point where the hexagonal flat sides disappeared into the rounder corners, and the nose was circular in cross section upstream of this point with a spherical segment at the stagnation point.

The tank is instrumented with 136 temperature transducers arranged at the locations specified in table I. No. 30 gage (0.0254-cm diameter) chromel-alumel thermocouple wires are spotwelded to the surface at each station, and the insulated dual cable leads extend through the sting to a terminal board outside the tunnel. The thickness of the model was measured at each temperature station. This thickness varied from 0.0762 cm to 0.0826 cm.

The orbiter model is shown in figure 2. Aerodynamic characteristics and details of the configuration and its construction were previously reported in reference 5. The orbiter was solid cast aluminum and not instrumented to measure heating rates. A photograph of the mated configuration as installed in the wind tunnel appears in figure 3. The mated models were considered alined when the top line of the orbiter was parallel to the axis of the tank. The sliding collars allow axial and radial adjustment of the orbiter position. In addition, the tank could be rotated so that either the flat side or the round side was adjacent to the orbiter. The removable door for the installation and inspection of thermocouples in the tank is in view.

Facility

The models were tested in the Langley continuous-flow hypersonic tunnel which can be operated continuously or in a blowdown mode (refs. 6 and 7). The three-dimensional nozzle has a 78.7-cm-square test section. The air is heated to approximately 980 K to prevent liquefaction in the expansion region. A model injection mechanism mounted on the side of the test section allowed the models to be quickly injected into and withdrawn from the test region. The tunnel was operated in a blowdown mode during the present tests.

Methods and Test Conditions

The heat transfer to the tank was determined from the transient temperature change in the model skin shortly after the model was injected into the airstream. The model was withdrawn after several seconds and cooled for the next run. An isothermal condition of the skin was assured prior to each injection by monitoring the skin temperatures.

The output of the thermocouples was measured by high-resistance fast-response galvanometers and recorded on magnetic tape at the rate of 20 samples per second. First evidence of model entry into the test airstream was the stagnation point temperature rise. Passage of the test model into the test region required no more than 0.3 sec. Rates of temperature change used in heat transfer determination varied from about 210 K/sec down to below 0.5 K/sec. Data from both extremes of this range were examined to determine the beginning of transient temperature change for calculation of the heating rates. This time started approximately 0.5 sec after the first indication of model entry into the tunnel.

The heat transfer coefficients at the temperature transducer stations were calculated from

$$h = \frac{\rho_m c_p t \frac{\partial T_w}{\partial \tau}}{T_{aw} - T_w}$$

The rate of temperature rise $\partial T_w/\partial \tau$ was determined from the derivative of a second degree polynomial least squares fit to 1 sec of data. Comparison of experimental data with theory at the nose indicated negligible conduction effects. Total temperature was used for adiabatic wall temperature because of inaccurate knowledge of local flow conditions in the interference flow field. The heat transfer at all stations was nondimensionalized with respect to the theoretical heating rate at the stagnation point of a reference sphere of radius 0.171 cm as determined by the method of Fay and Riddell (ref. 8).

All configurations were tested at the same nominal physical conditions and all data were reduced by using a free-stream Mach number value of 10.3. The stagnation pressure was approximately 5.2 MN/m^2 and the stagnation temperature was approximately 980 K. The nominal free-stream unit Reynolds number was 3.3×10^6 per meter.

The control variables in this parametric study are (1) a position with the orbiter mated to the round side of the tank as compared with a position 180^o from this with the orbiter mated to the flat side, (2) a position with the orbiter mated to a side of the tank with zero gap spacing as compared with two other gap spacings, (3) a position with the orbiter mated to a side of the tank at 0^o angle of attack as compared with 5^o angle of attack, and (4) a position with the orbiter mated to a side of the tank at a central axial location as compared with a location upstream of this location and another downstream of this location, as shown in figure 4. All possible combinations of the preceding control variables including 3 without any orbiter interference add up to a total test grid of 39 test configurations. The test grid covered in this investigation, which includes 14 configurations, is listed in table II, and these data are shown in figures 5, 6, and 7. Important details of these figures are shown in table II. All the data obtained in the present investigation are presented in figures 5, 6, and 7. Comparison of selected rays from the aforementioned data is presented in figures 8 to 17 and details of this comparison are outlined in table III.

RESULTS AND DISCUSSION

Heat Transfer to Tank Alone

The heat transfer to the tank alone, shown in figure 5, tended toward lower values at stations progressively distant from the nose, as expected for laminar flow. The data

are compared with a laminar two-dimensional axisymmetric heat transfer theory (ref. 9). The pressure used in the computation of this laminar theory was output from a three-dimensional flow field calculation (ref. 10), which provided velocities between the body surface and the shock and provided consequent pressure distributions along each ray. Slightly different pressure distributions along the round and the flat sides account for the slight difference in the two theoretical heat transfer distributions.

The theory agrees with the general trend of the data to a value of $l/L = 0.6$ or $l/L = 0.7$, although the theory is about a factor of two below the data. For the region from $l/L = 0.6$ to the end, the theory does not agree with the trend of the data very well, although it agrees better with the general level of the data. The local physical flow phenomena responsible for the extreme gradients in heat transfer toward the base are not understood. It is possible that extraneous test flows have an effect. The test results, however, have been carefully examined for the normally expected errors, and there seems little excuse to discard any of it. In any case, fairing the data as shown in this report does not alter the basic conclusions of the report.

Heat Transfer to Tank With Orbiter Mated

The shock interference heating pattern on the surface of the tank was determined with the orbiter in various positions near the tank. The heat transfer measured with the orbiter mated to the round side of the tank is shown in figure 6, and that measured with the orbiter mated to the flat side is shown in figure 7.

The shock interference patterns produced by the initially intersecting shocks, followed subsequently by downstream reflections and interactions, play an important part in the measured heat transfer between the mated vehicles. A study of the types of shock interaction affecting the present tests is shown in figures 18, 19, 20, and 21. The shock interaction pattern most prevalent throughout this series of tests is that shown in figure 18. It occurs for $\Delta/L = 0$ and $\Delta/L = 0.17$ and falls into the category of the Edney type I intersection pattern (ref. 1). For the orbiter at these two forward axial locations, the type of shock intersection pattern was unaffected by the angle-of-attack changes of this series of tests.

The schlieren or shadowgraph photographs are of poor quality.[2] Nevertheless, they suggest the presence of three other types of shock interaction. When the orbiter is in the rearmost axial location ($\Delta/L = 0.34$) at 0° angle of attack, the intersecting shocks apparently form either an Edney type III or type IV interaction. These types are illustrated in figures 19 and 20. When the orbiter is in the rearmost position at 5° angle of

[2]The shadowgraph or schlieren photographs were taken using a mirror on the injection plate surface. Although the hot quartz window on the other side of the tunnel severely distorted the picture, several types of shock patterns were identifiable.

attack, the shock from the tank strikes the orbiter nose at a higher position, probably producing an Edney type V shock interaction pattern. This is shown in figure 21. The types of shock interaction near the nose of the orbiter have a direct effect on the heat transfer to the orbiter nose, but a secondary effect should be observed on the surface of the tank.

To allow a systematic appraisal of the data, results obtained at all heat transfer stations are shown in each part of figures 6 and 7, but only the rays adjacent to the orbiter position ($\phi = -90^{o}$ in fig. 6; $\phi = +90^{o}$ in fig. 7), opposite the orbiter position ($\phi = +90^{o}$ in fig. 6; $\phi = -90^{o}$ in fig. 7), and 90^{o} away from the orbiter position ($\phi = 0^{o}$) have been faired. The ordinate h/h_{ref} covers a range from 0.001 to 1.0. The axial location of the minimum distance between the two vehicles is shown for all mated heat transfer tests. The shock interference heat transfer data shown in figure 6 with the orbiter mated to the round side of the tank show that regions of extremely high heat transfer exist along the adjacent ray ahead of the minimum gap. The interference effect along this ray produced a heat transfer signature with sharp peaks and valleys. The heat transfer signatures along the other two faired rays also have peaks and valleys, but the maximum heat transfer increase along these rays was less, and the peaks and valleys were less sharp.

The characteristic peaks and valleys of the heat transfer signatures suggest complicated local flow phenomena indicative of shock—boundary-layer interactions. The heat transfer data along rays other than those faired often fall between the data on faired rays or are at least in the general neighborhood of these data. In some test configurations, however, part of the intervening data show widely divergent values. Some cases of special interest are those in which heat transfer coefficients an order of magnitude above the adjacent data occur along the $\phi = 41.5^{o}$ ray at stations approaching the base of the model. (See figs. 6(b), 6(d), 6(g), and 6(h).) Similar phenomena happen along the side ray ($\phi = 0^{o}$) in figures 6(e) and 6(f). Such interference results have been observed previously in phase change data of a booster-orbiter combination (e.g., ref. 4, p. 359).

The data presented in figure 7 for the orbiter mated to the flat side of the tank show shock interference heat transfer patterns similar to those observed for the round side mated to the orbiter (fig. 6). Fewer cases were studied with the flat side mated to the orbiter since no tests were made at 5^{o} angle of attack. The overall data for the flat side mated to the orbiter appear slightly different from the data for the round side mated to the orbiter, but in this form, no consistent outstanding differences are noted.

Effect of Longitudinal Position

Adjacent instrumentation ray.- The heat transfer to the adjacent ray for the three longitudinal positions of the orbiter is presented in figures 8(a), 8(b), and 8(c) and compared with the no-interference heat transfer in figures 8(a) and 8(c). These results show the heat transfer for the round side of the tank mated to the orbiter at $\alpha = 0^{o}$

and $\alpha = 5^{o}$ and for the flat side of the tank mated to the orbiter at $\alpha = 0^{o}$. This heat transfer has many points of similarity for the two sides and the two angles of attack. The reduction of the heat transfer to below the no-interference values ahead of the initial shock impingement on the tank is evidence of an adverse pressure gradient leading to possible separation (ref. 11). Immediately behind these reduced values, the heat transfer climbs to peak values two orders of magnitude greater than the no-interference case with a second peak downstream from the first peak. In the case of $\Delta/L = 0.34$ (the rearmost position), the second peak is more of a plateau of high-level heating. The twin peak heat transfer signature is located at three axial positions on the adjacent ray for the three mated positions of the orbiter alongside the tank.

In the case where the orbiter is in the most upstream position ($\Delta/L = 0$), the heat transfer reaches a downstream peak value from approximately a factor of 2 to a factor of 3 above the upstream peak value. Although the quantity of data does not absolutely define the shape of these peaks, they are probably close to the same sharpness. The type of shock reflection causing this shape of heat transfer signature is suggested by the shock pattern identified in a photographic study of the flow field, an example of which is shown in the left photograph of figure 18. This shock pattern is also illustrated in the schematic of figure 18. The bow wave from the orbiter nose strikes the tank, is reflected to and from the orbiter, and strikes the tank a second time at approximately the same place that the reflected bow wave from the tank nose strikes the tank. This concentrated double shock or possible λ shock effect may well explain the increased heating at the location of the second peak.

On the other hand, when the orbiter is in the central position ($\Delta/L = 0.17$), the first heat transfer peak reaches the greater maximum heat transfer level except when the flat side is mated, and in this case, the comparative maxima are not rigorously defined by the data. Another obvious change in the heat transfer signature is the flattened second peak. The photographic evidence of the shock pattern produced by this tank-orbiter configuration suggests a coincident impingement of the orbiter nose shock and the reflection of the tank nose shock upon the tank surface at the position of the first peak. Downstream of the intersection of the two shocks seen in the right photograph of figure 18, the surfaces of the mated vehicles are closer together for $\Delta/L = 0.17$ than for $\Delta/L = 0$, and the shock pattern becomes less distinct. This probably accounts for the flattened second peak.

When the orbiter is in the most downstream position relative to the tank, the bow shock from the tank strikes the bow shock from the orbiter near the nose, and any traces of it downstream from this disappear quickly. The position where the bow shock from the orbiter strikes the tank is the same as the position of peak heating observed for this case in figure 8.

Side and opposite rays.- The heating along the side ray is affected by interference as shown in figures 9(a), 9(b), and 9(c). Heat transfer peaks and valleys caused by a shock pattern wrapped around the tank are clearly evident. The shock from the orbiter wing must enter into the development of this pattern. Part of the heat transfer pattern may be attributed to transitional boundary-layer flow. For the round side mated to the orbiter at $\alpha = 0^{o}$ (fig. 9(a)), the first peak follows the position of the orbiter downstream. The interference effect occurs at a lower heating level, but the heat transfer variation caused by the aft movement of the orbiter (from $\Delta/L = 0$ to $\Delta/L = 0.34$) increases the heat transfer at one station by more than an order of magnitude $\left(\text{from } h/h_{ref} = 0.002 \text{ to } h/h_{ref} = 0.06\right)$. With the round side mated to the orbiter at $\alpha = 5^{o}$ (fig. 9(b)), the position of the first peak moves much less with translation of the orbiter than at $\alpha = 0^{o}$, and the shape of the heating distribution appears to be that for transition to turbulence. With the flat side mated to the orbiter (fig. 9(c)), the heat transfer signature is more like that shown in figure 9(a) but with less drastic heat transfer changes.

The heat transfer along the opposite ray is shown in figures 10(a), 10(b), and 10(c). The interference effect occurs further downstream and the heat transfer rises toward the base for both cases at $\alpha = 0^{o}$. The interference effect is similar for the round side mated to the orbiter and for the flat side mated to the orbiter at $\alpha = 0^{o}$ but is more pronounced for the latter case. At $\alpha = 5^{o}$ with the round side mated to the orbiter, the interference effect on heat transfer is much less evident. This is to be expected since the peripheral flow induced by the angle of attack is such as to oppose that induced by the orbiter interference. The opposite ray interference effect resembles the effect of transition for the cases at $\alpha = 0^{o}$. If transition is present, it occurs at an unusually low Reynolds number since the free-stream Reynolds number of the flow is only 10^{6} based on L the length of the tank.

Effect of Gap

The effect of a gap on the interference heat transfer is shown in figure 11 for the orbiter on the round side of the tank. The two minimum gaps used were 0.051 cm and 0.102 cm. Tests for the effect of the gap were all performed with the orbiter in the center axial position ($\Delta/L = 0.17$) of the three positions.

The heat transfer along the adjacent ray for the orbiter on the round side of the tank (fig. 11(a)) is reduced in the interference region ahead of the minimum gap by an increase in the gap, and this reduction is nearly a linear function of gap spacing. Downstream of the minimum gap, however, the opposite effect is observed; the heat transfer is increased by an increase in gap. Since the average level of the data downstream of the minimum gap is more than an order of magnitude below that ahead of the gap, the effect of the gap is of less importance in this region.

The heat transfer to the side ray and to the opposite ray with the gap is shown in figures 11(b) and 11(c). The heat transfer to the side ray is reduced by an increase in the gap size, while the heat transfer to the opposite ray is increased by an increase in the gap size. The heat transfer is at such a low level that its effect is of less importance than in the higher heat transfer zones, but the change in heating ranges to nearly 100 percent. This illustrates the far-reaching effect of the "dead air" space between the vehicles and how the effective shape of the mated configuration is changed with a small change in relative position of the two bodies.

The effect of the gap on the interference heat transfer with the orbiter on the flat side of the tank is shown in figure 12. Again, the heat transfer was reduced by the gap increase in the region ahead of the minimum gap and was increased by the gap increase in the region downstream from the minimum gap along the adjacent ray. The agreement between the data for δ/L of 0.0017 and for δ/L of 0.0034 is striking.

Effect of α

A mated configuration was tested at 5° angle of attack only for the round side mated to the orbiter with no gap. The effect of a change in α from 0° to 5° is shown in figures 13, 14, and 15. The effect of α on the tank ray adjacent to the orbiter in all three axial locations is shown in figure 13. In the nose region before the start of interference, the heat transfer is reduced by the increase in α as the measured surface becomes the lee side. From the start of the interference region to the position of the minimum gap, the heat transfer is changed only slightly by the change in α except when the orbiter is in the rearmost axial position. In this position, the type of shock interference at the nose of the orbiter was affected by the angle-of-attack change as previously discussed in figures 18, 19, 20, and 21. Figure 13(c) indicates that energy was diverted by the angle-of-attack change from a streamline under the vehicle to a streamline above the vehicle as is indicated by the diagrams in figures 19, 20, and 21.

The effect of α on the side ray of the tank is observed in figure 14. Here, the effect is large although it is at a low level. When the orbiter is in the center position, the angle-of-attack variation changes the heat transfer values an order of magnitude at several stations. This is probably caused by a change in position of one of the localized high heating zones previously discussed.

The effect of angle of attack on interference heat transfer to the opposite ray is shown in figure 15. At this location, the heat transfer to the entire ray increases with α as expected and is not a result of the mated body interferences. The wraparound of the interference may cause the waviness observed in some parts of figure 15, and the interference on this ray is probably responsible for part of the apparent transition on this ray.

Comparison for Round and Flat Side Mating

Comparison of the interference heating on the flat side of the tank with that on the round side of the tank is made for the orbiter in the center of the three axial positions. The effect of the interference is compared for the adjacent ray and for the side ray.

The adjacent rays are compared in figure 16. Ahead of the interference region, the data agree with the previously obtained no-interference data. Over the remainder of the tank, the interference heat transfer for the flat side is greater than that for the round side. Not only is the heat transfer higher on the flat side, but it has also increased more since the flat side had lower local heating with no interference.

The side ray data are compared in figure 17. The shock-induced flow influences the heat transfer on the side ray farther forward when the flat side is mated to the orbiter. The comparison of the heating on the side ray shows moderate changes in heat transfer at a low level.

CONCLUDING REMARKS

The aerothermodynamic effect of shock interference on an external tank mated with a straight-wing shuttle orbiter has been studied at a Mach number of 10.3 and at a free-stream Reynolds number of 10^6 based on the tank length. Local heat transfer has been determined from transient thin-skin temperature measurements examined when an isothermal skin condition precluded lateral skin conduction considerations. The investigation was a parametric study of shock interference heat transfer for two mated bodies with the relative longitudinal position, the angle of attack, the gap, and the cross-section shape of the tank (cylindrical or flat) adjacent to the orbiter as control variables.

Comparison of interference heat transfer with no-interference heat transfer shows that shock interference can increase the heat transfer by two orders of magnitude along the adjacent ray of the tank. The heat transfer signature along this ray showed extremely sharp peaks and valleys. Transducer rays progressively further from the orbiter disclosed lower interference effects, but interference effects as great as an order of magnitude occurred even on the opposite ray.

The locations of the extremely sharp peaks and valleys of heat transfer along the adjacent ray are directly affected by the relative axial location of the two mated vehicles. The effects of angle of attack, gap, and cross-section shape were evident but were not as consistent or as extreme.

Langley Research Center
National Aeronautics and Space Administration
Hampton, Va. 23665
March 8, 1976

REFERENCES

1. Edney, Barry: Anomalous Heat Transfer and Pressure Distributions on Blunt Bodies at Hypersonic Speeds in the Presence of an Impinging Shock. FFA Rep. 115, Aeronaut. Res. Inst. of Sweden, 1968.

2. Keyes, J. Wayne; and Hains, Frank D.: Analytical and Experimental Studies of Shock Interference Heating in Hypersonic Flows. NASA TN D-7139, 1973.

3. Brevig, O.; and Young, C.: Shock Interference Heating on the Space Shuttle Booster During Ascent. NASA Space Shuttle Technology Conference. Volume I – Aerothermodynamics, Configurations, and Flight Mechanics. NASA TM X-2272, 1971, pp. 245-266.

4. Edney, Barry E.: Shock Interference Heating and the Space Shuttle. Space Transportation System Technology Symposium, NASA TM X-52876, Vol. I, 1970, pp. 338-389.

5. Stone, David R.: Aerodynamic Characteristics of a Fixed-Wing Manned Space Shuttle Concept at a Mach Number of 6.0. NASA TM X-2049, 1970.

6. Schaefer, William T., Jr.: Characteristics of Major Active Wind Tunnels at the Langley Research Center. NASA TM X-1130, 1965.

7. Dunavant, James C.; and Stone, Howard W.: Effect of Roughness on Heat Transfer to Hemisphere Cylinders at Mach Numbers 10.4 and 11.4. NASA TN D-3871, 1967.

8. Fay, J. A.; and Riddell, F. R.: Theory of Stagnation Point Heat Transfer in Dissociated Air. J. Aeronaut. Sci., vol. 25, no. 2, Feb. 1958, pp. 73-85, 121.

9. Anderson, E. C.; and Lewis, C. H.: Laminar or Turbulent Boundary-Layer Flows of Perfect Gases or Reacting Gas Mixtures in Chemical Equilibrium. NASA CR-1893, 1971.

10. Marconi, Frank; Yaeger, Larry; and Hamilton, H. Harris: Computation of High-Speed Inviscid Flows About Real Configurations. Aerodynamic Analyses Requiring Advanced Computers – Part II, NASA SP-347, 1975, pp. 1411-1455.

11. Chapman, Dean R.; Kuehn, Donald M.; and Larson, Howard K.: Investigation of Separated Flows in Supersonic and Subsonic Streams With Emphasis on the Effect of Transition. NACA Rep. 1356, 1958. (Supersedes NACA TN 3869.)

TABLE I.- LOCATION OF TEMPERATURE TRANSDUCERS ON MODEL SKIN

Axial location, l, cm	Transducer location at ϕ of –									
	-90°	-67.5°	-45°	-22.5°	0°	20.7°	41.5°	60°	74.7°	90°
0	✓	✓	✓	✓	✓	✓	✓	✓	✓	✓
1.27	✓	✓		✓		✓		✓		✓
2.54	✓		✓		✓		✓		✓	✓
3.81	✓	✓		✓		✓		✓		✓
5.08	✓		✓		✓		✓		✓	✓
6.35	✓	✓		✓		✓		✓		✓
7.62	✓		✓		✓		✓		✓	✓
8.89	✓	✓		✓		✓		✓		✓
10.16	✓		✓		✓		✓		✓	✓
11.43	✓	✓		✓		✓		✓		✓
12.70	✓		✓		✓		✓		✓	✓
13.97	✓	✓		✓		✓		✓		✓
15.24	✓		✓		✓		✓		✓	✓
16.51	✓	✓		✓		✓		✓		✓
17.78	✓		✓		✓		✓		✓	✓
19.05	✓	✓		✓		✓		✓		✓
20.32	✓		✓		✓		✓		✓	✓
21.59		✓		✓		✓		✓		✓
22.86	✓		✓		✓		✓		✓	
24.13		✓		✓		✓		✓		✓
25.40	✓		✓		✓		✓		✓	
26.67		✓		✓		✓		✓		✓
27.94	✓		✓		✓		✓		✓	

TABLE II.- COMPLETE GRAPHICAL PRESENTATION OF CONTROL VARIABLES UTILIZED IN THE PRESENT REPORT

Figure	Mated side of tank	Angle of attack, α, deg	Axial position, Δ/L	Gap, δ/L
5	No orbiter	0	---	-----
6(a)	Round	0	0.00	0.0000
6(b)		0	.17	
6(c)		0	.34	
6(d)		5	0.00	
6(e)		5	.17	
6(f)		5	.34	
6(g)		0	.17	.0017
6(h)		0	.17	.0034
7(a)	Flat	0	0.00	0.0000
7(b)			.17	
7(c)			.34	
7(d)			.17	.0017
7(e)			.17	.0034

TABLE III.- COMPARATIVE GRAPHICAL PRESENTATION OF INTERFERENCE HEAT TRANSFER CONTROL VARIABLES

Figure	Control variable	Mated side	Angle of attack, α, deg	Axial position, Δ/L	Gap, δ/L	Circumferential ray, ϕ, deg
8(a)	Axial position	Round	0	Variable	0	-90 (adjacent)
8(b)		Round	5			-90 (adjacent)
8(c)		Flat	0			+90 (opposite)
9(a)	Axial position	Round	0	Variable	0	0 (side)
9(b)		Round	5			
9(c)		Flat	0			
10(a)	Axial position	Round	0	Variable	0	+90 (opposite)
10(b)		Round	5			+90 (opposite)
10(c)		Flat	0			-90 (adjacent)
11(a)	Gap	Round	0	0.17	Variable	-90 (adjacent)
11(b)						0 (side)
11(c)						+90 (opposite)
12(a)	Gap	Flat	0	0.17	Variable	-90 (adjacent)
12(b)						0 (side)
12(c)						+90 (opposite)
13(a)	Angle of attack	Round	Variable	0.00	0	-90 (adjacent)
13(b)				.17		
13(c)				.34		
14(a)	Angle of attack	Round	Variable	0.00	0	0 (side)
14(b)				.17		
14(c)				.34		
15(a)	Angle of attack	Round	Variable	0.00	0	+90 (opposite)
15(b)				.17		
15(c)				.34		
16(a)	Mated side	Variable	0	0.00	0	Variable (adjacent)
16(b)				.17		
16(c)				.34		
17(a)	Mated side	Variable	0	0.00	0	Variable (side)
17(b)				.17		
17(c)				.34		

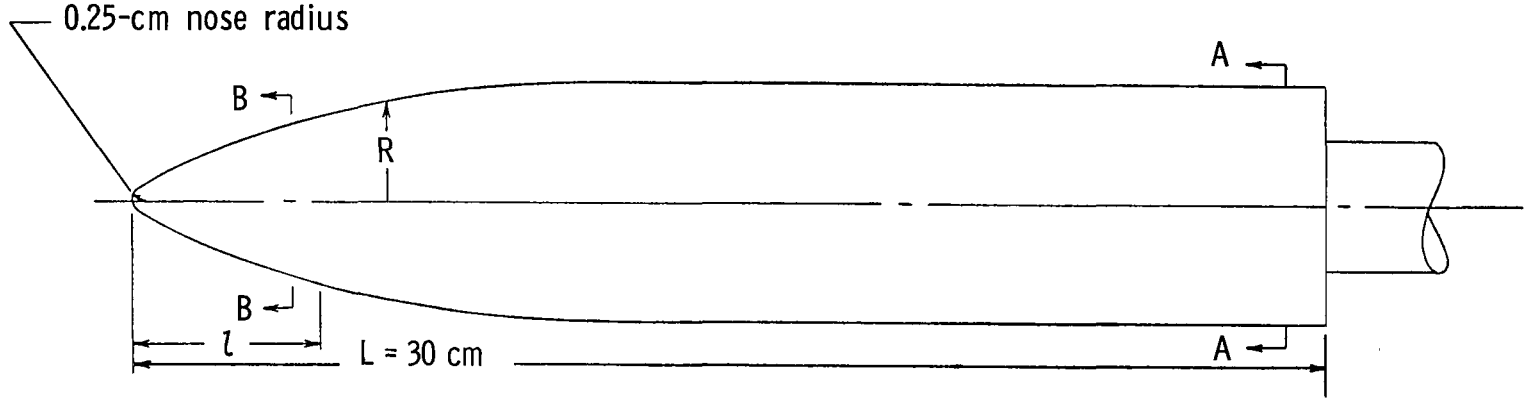

Coordinates of Nose (cm)

l	R
0	0
.50	.51
.75	.68
1.00	.82
1.50	1.04
2.00	1.23
2.50	1.41
4.00	1.86
5.50	2.25
7.00	2.56
8.50	2.82
10.00	2.97
12.00	3.00

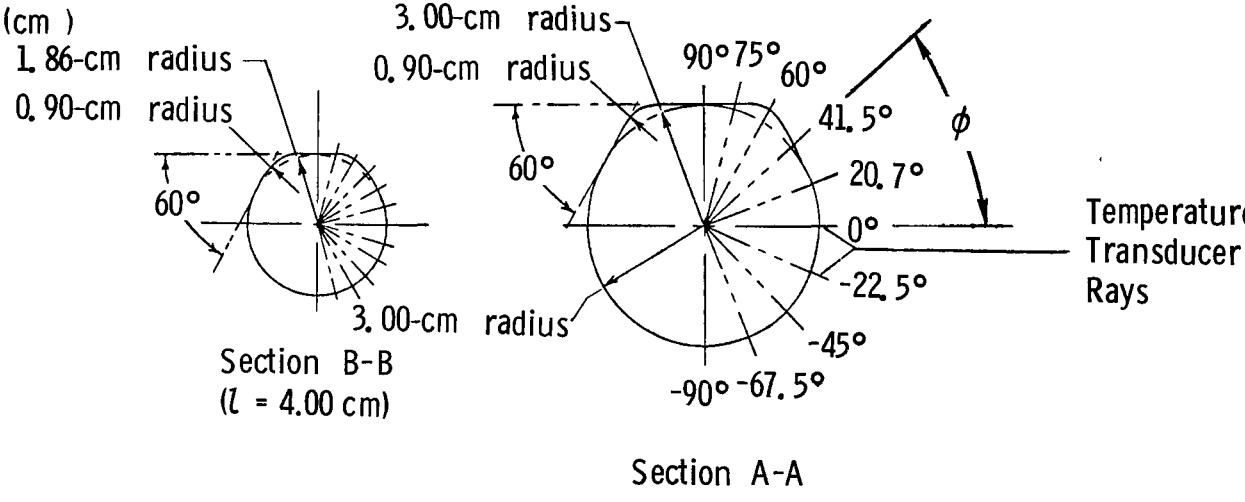

Figure 1.- Details of simulated tank.

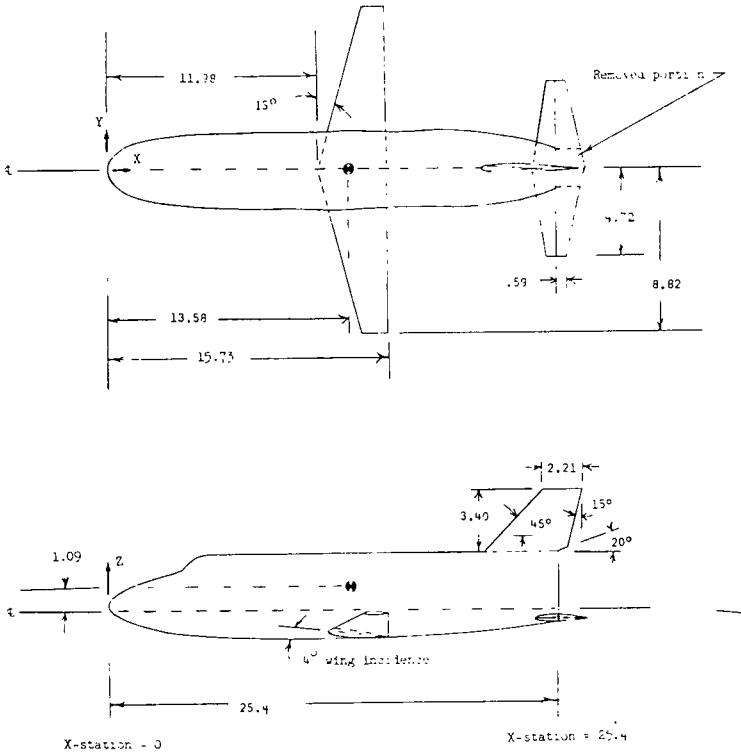

x/c	y/c
Horizontal tail (NACA 0012-64), center-line root chord, 2 98, tip chord, 1 05	
0 10	0 04
40	06
80	.03
1 00	001
Leading-edge radius, 0 06	Leading-edge radius, 0 02
Vertical tail (NACA 0012-64)	
z = 1 24, c = 6 12	z = 6 48; c = 2 21
0 10	0 04
40	.06
80	.03
1 00	.001
Leading-edge radius, 0 11	Leading-edge radius, 0.04

x/c	y/c
Wing root (NACA 0014-64), center-line root chord, 3 75	
0 15	0 06
.50	07
90	02
1.00	.002
Leading-edge radius, 0 06	
Wing tip (NACA 0010-64); tip chord, 1 33	
0.15	0 05
.50	.05
.90	.01
1.00	.005
Leading-edge radius, 0.02	

(a) General arrangement.

Figure 2.- Details of orbiter model. All linear dimensions are in centimeters.

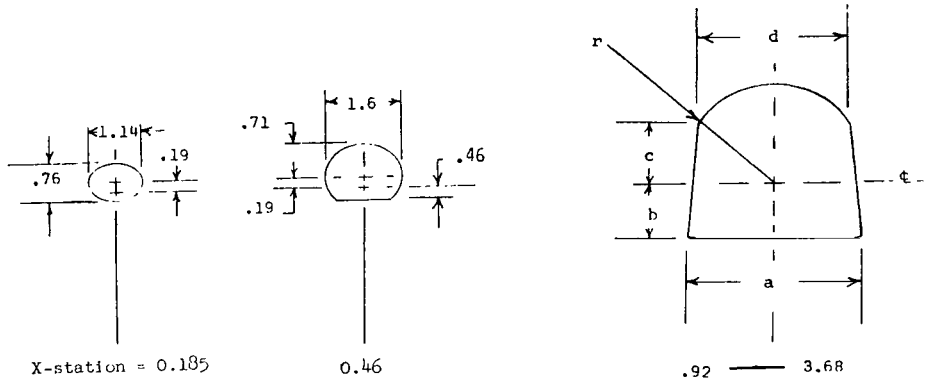

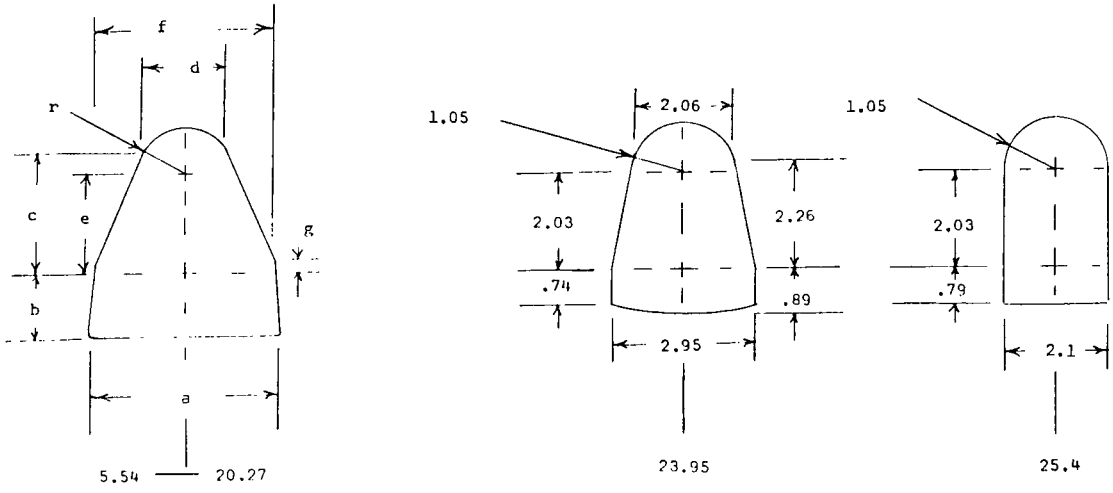

X-station	a	b	c	d	e	f	g	r
0.92	2.22	0.46	0.66	1.93				1.14
1.85	2.79	.73	1.02	2.11				1.47
2.76	3.25	.97	1.12	2.62				1.78
3.68	3.56	1.14	1.27	3.05				2.03
5.54	3.91	1.37	2.41	1.75	2.03	3.68	0.25	.99
7.37	4.06	1.42	2.49	1.91	2.03	3.81	.25	1.05
11.05	4.19	1.52	2.49	1.91	2.03	3.94	.29	1.05
13.82	4.14	1.63	2.49	1.91	2.03	3.94	.29	1.05
15.55	3.94	1.52	2.48	1.91	2.03	3.94	.29	1.05
20.27	3.94	1.21	2.48	1.91	2.03	3.94	.29	1.05

(b) Cross sections.

Figure 2.- Concluded.

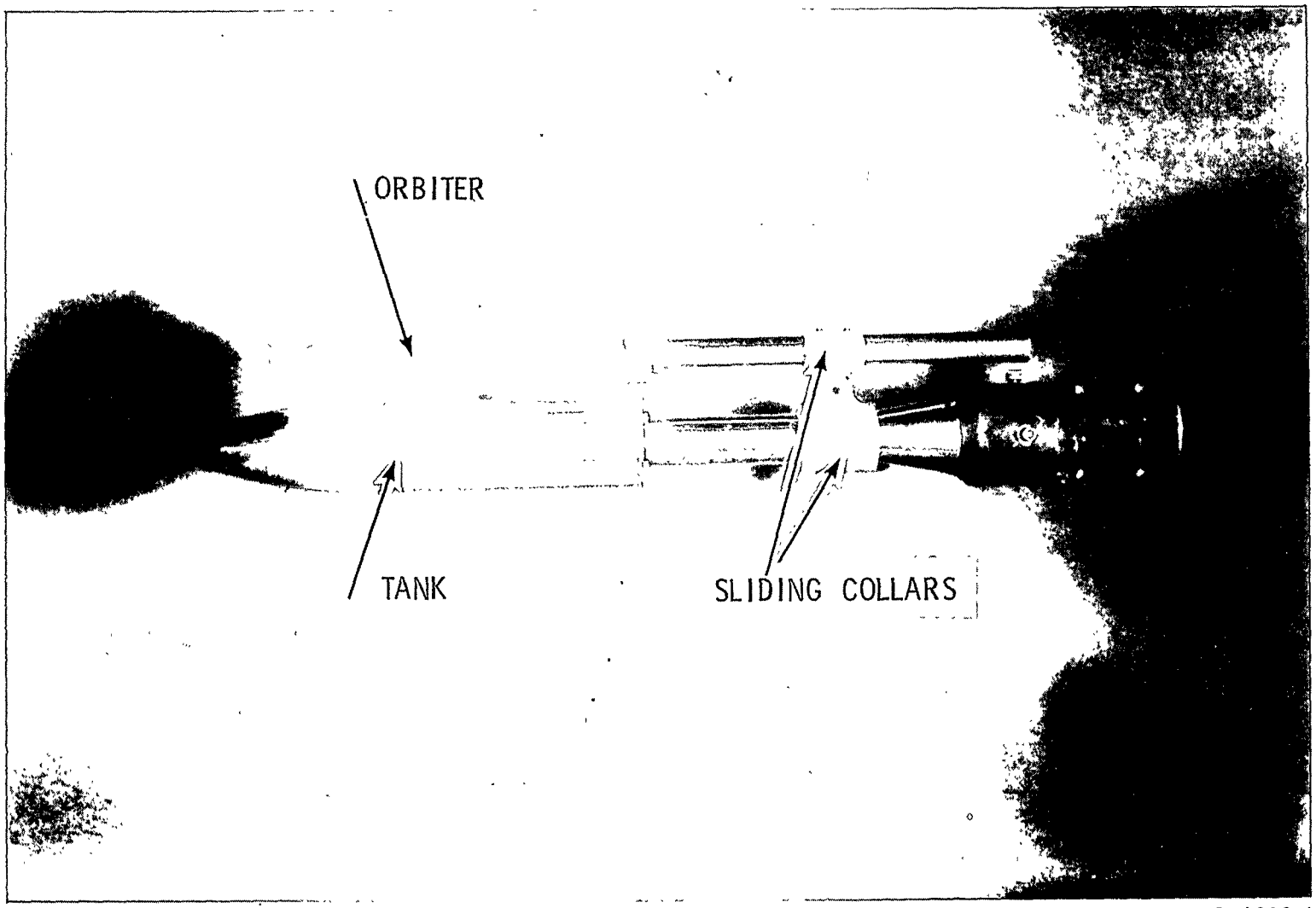

L-72-4636.1

Figure 3.- Photograph of orbiter-tank combination.

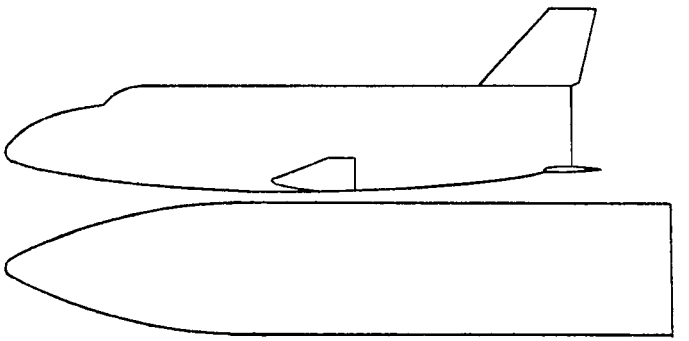

(a) $\Delta/L = 0.$

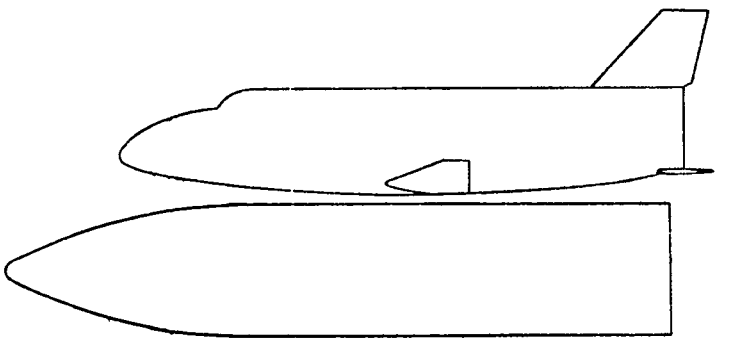

(b) $\Delta/L = 0.17.$

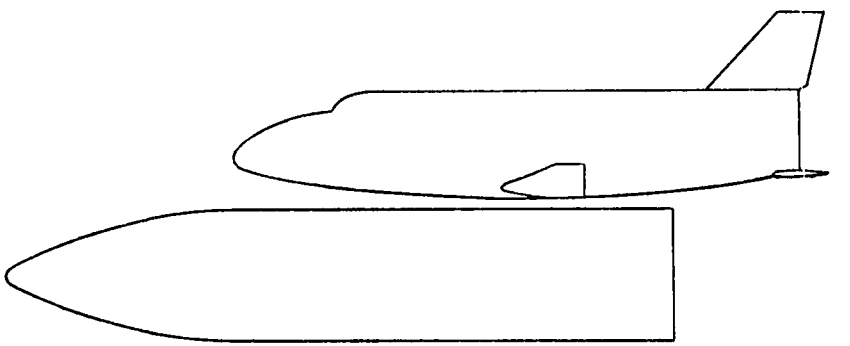

(c) $\Delta/L = 0.34.$

Figure 4.- Diagram of orbiter-tank combination.

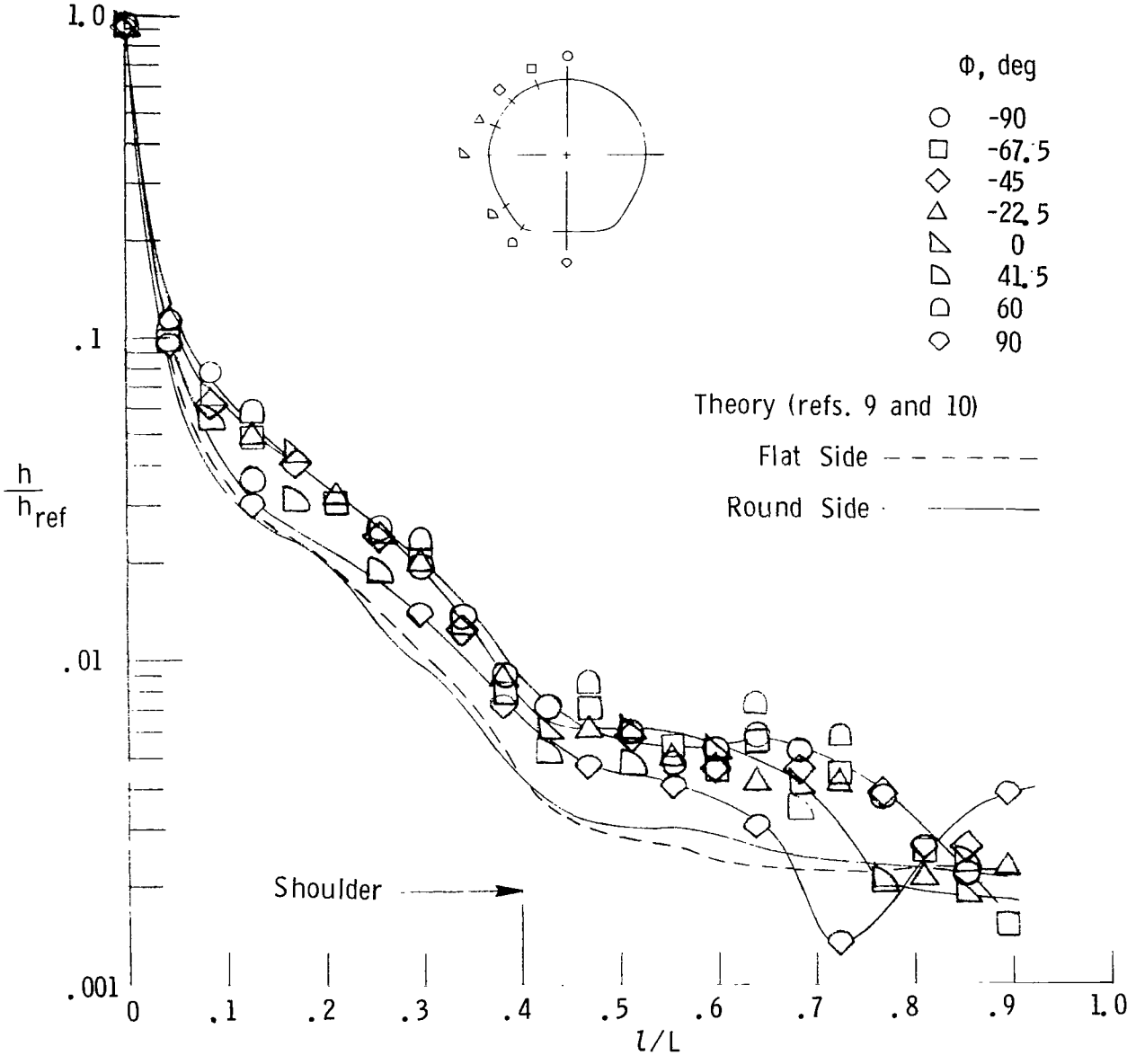

Figure 5.- Heat transfer to tank with no orbiter interference ($\alpha = 0^{o}$).

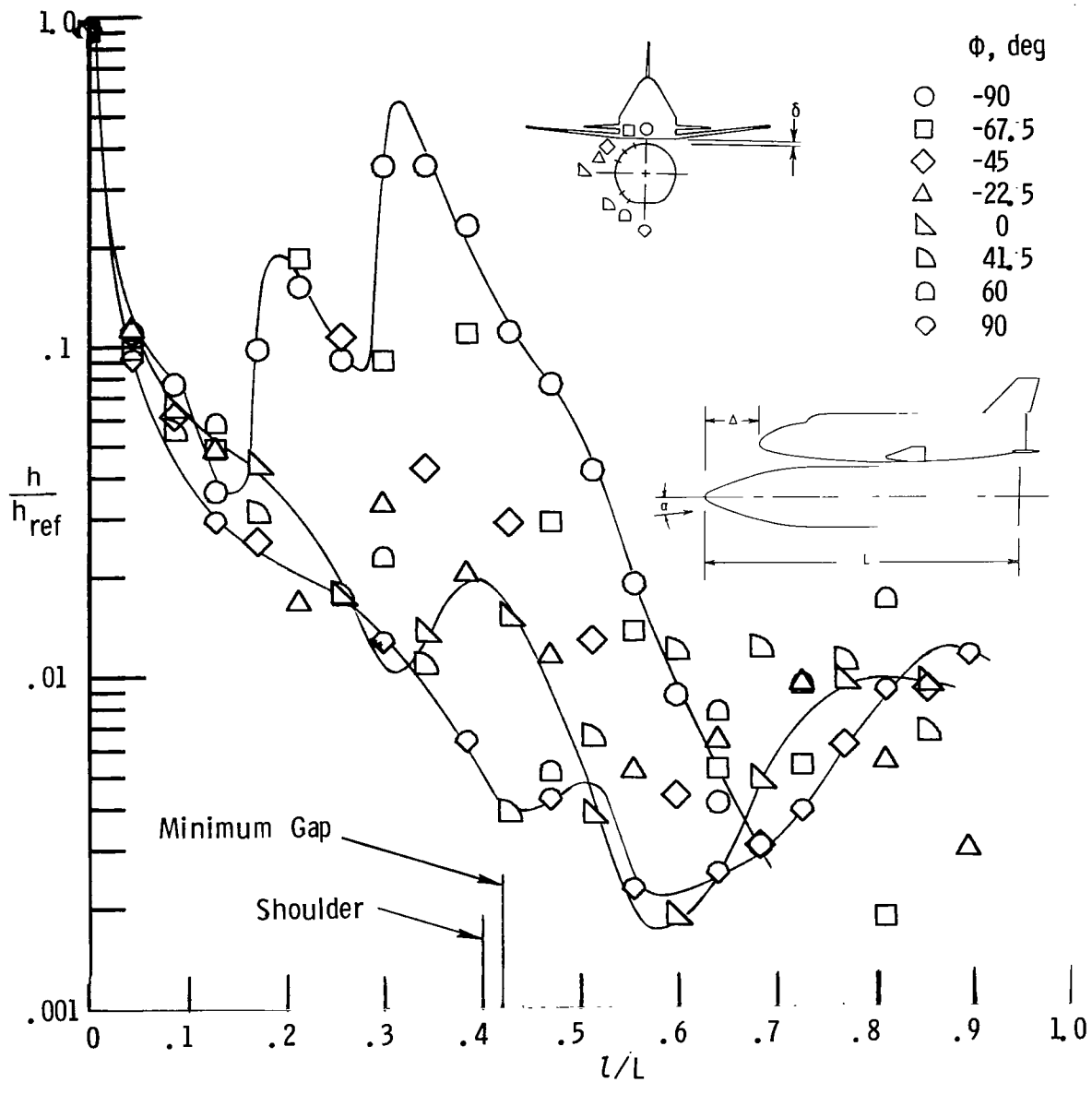

(a) $\alpha = 0^{o}$; $\delta/L = 0$; $\Delta/L = 0$.

Figure 6.- Heat transfer to tank with orbiter mated to round side.

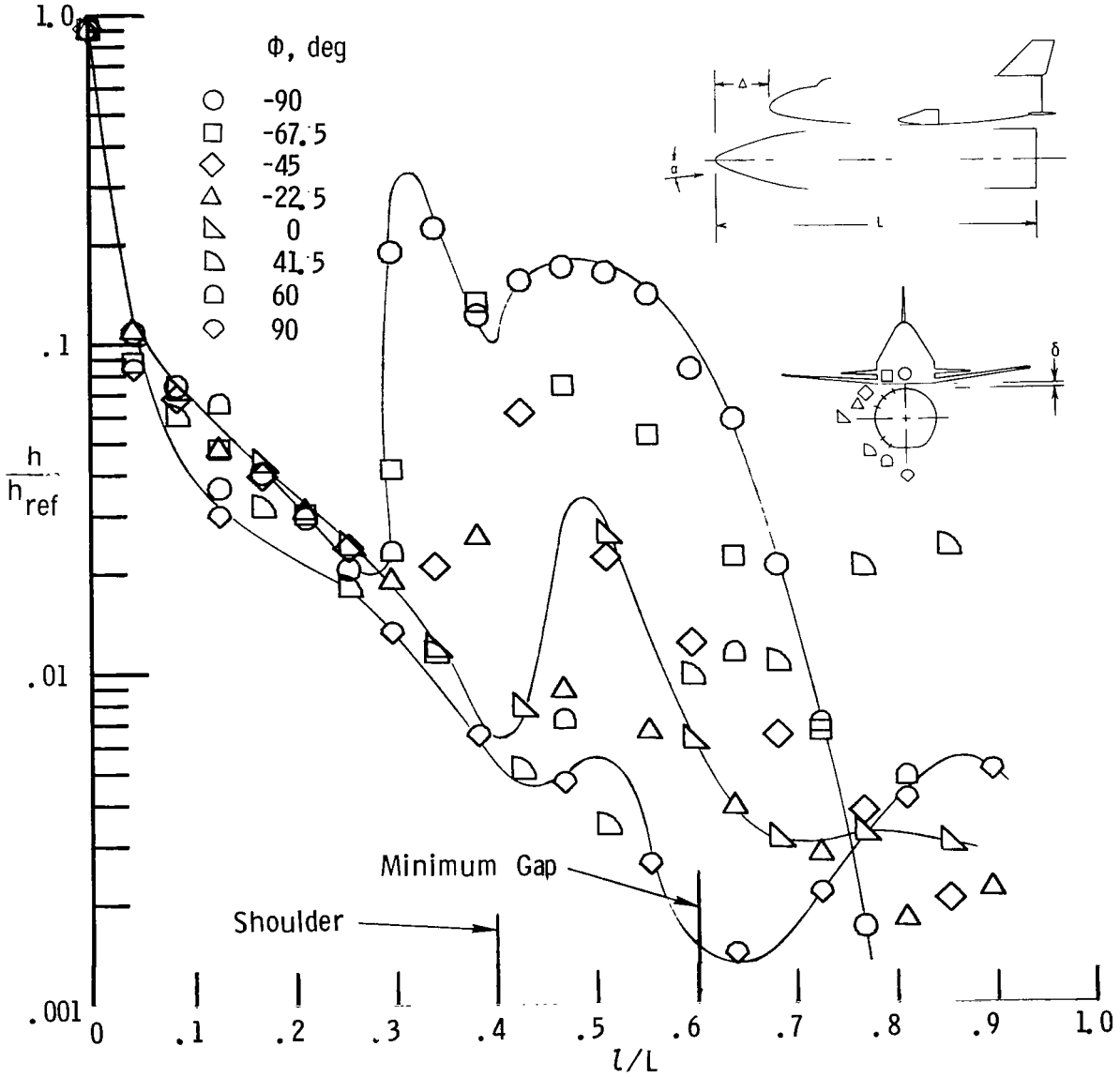

(b) $\alpha = 0^{o}$; $\delta/L = 0$; $\Delta/L = 0.17$.

Figure 6.- Continued.

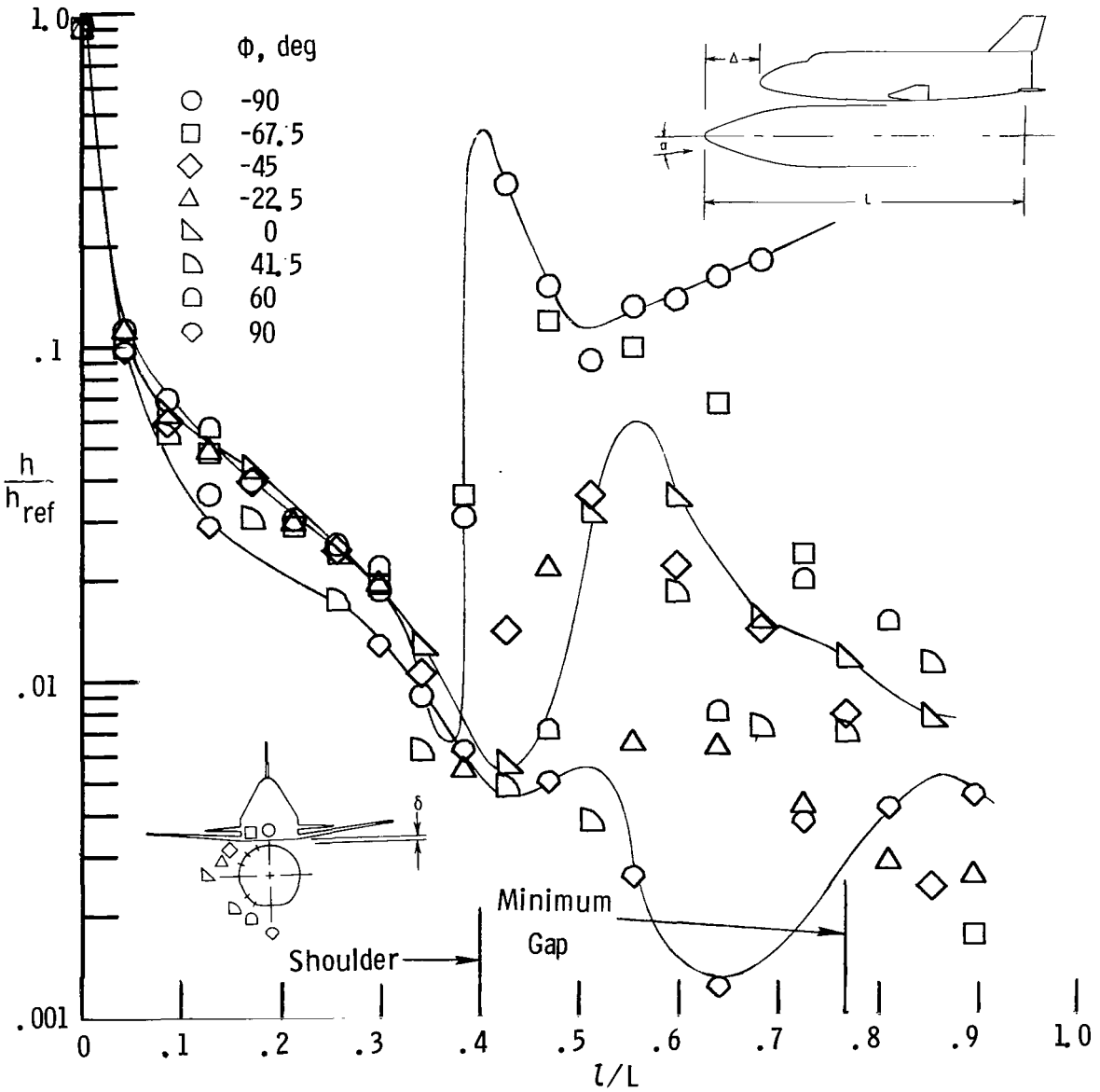

(c) $\alpha = 0^{o}$; $\delta/L = 0$; $\Delta/L = 0.34$.

Figure 6.- Continued.

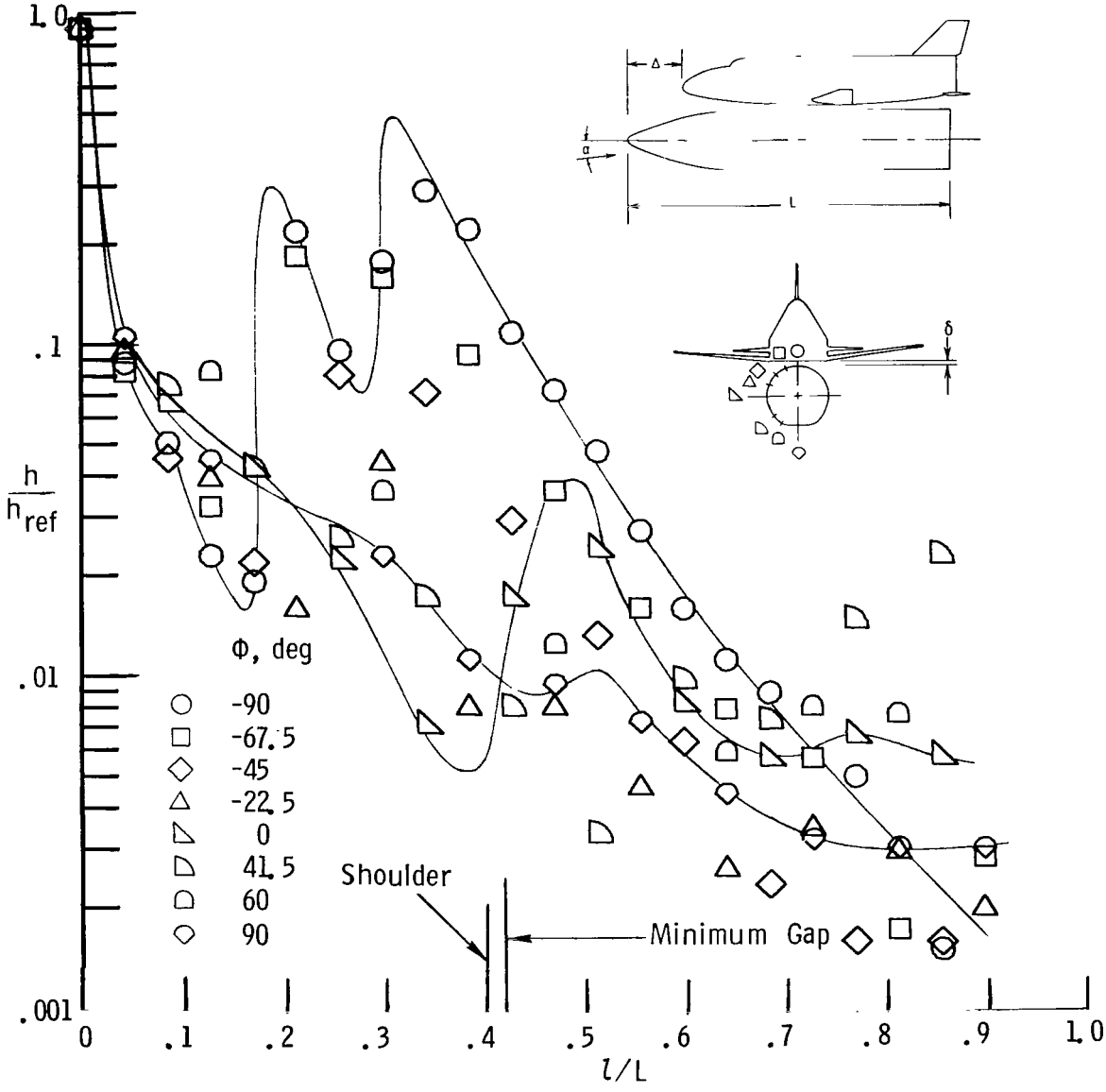

(d) $\alpha = 5^{o}$; $\delta/L = 0$; $\Delta/L = 0$.

Figure 6.- Continued.

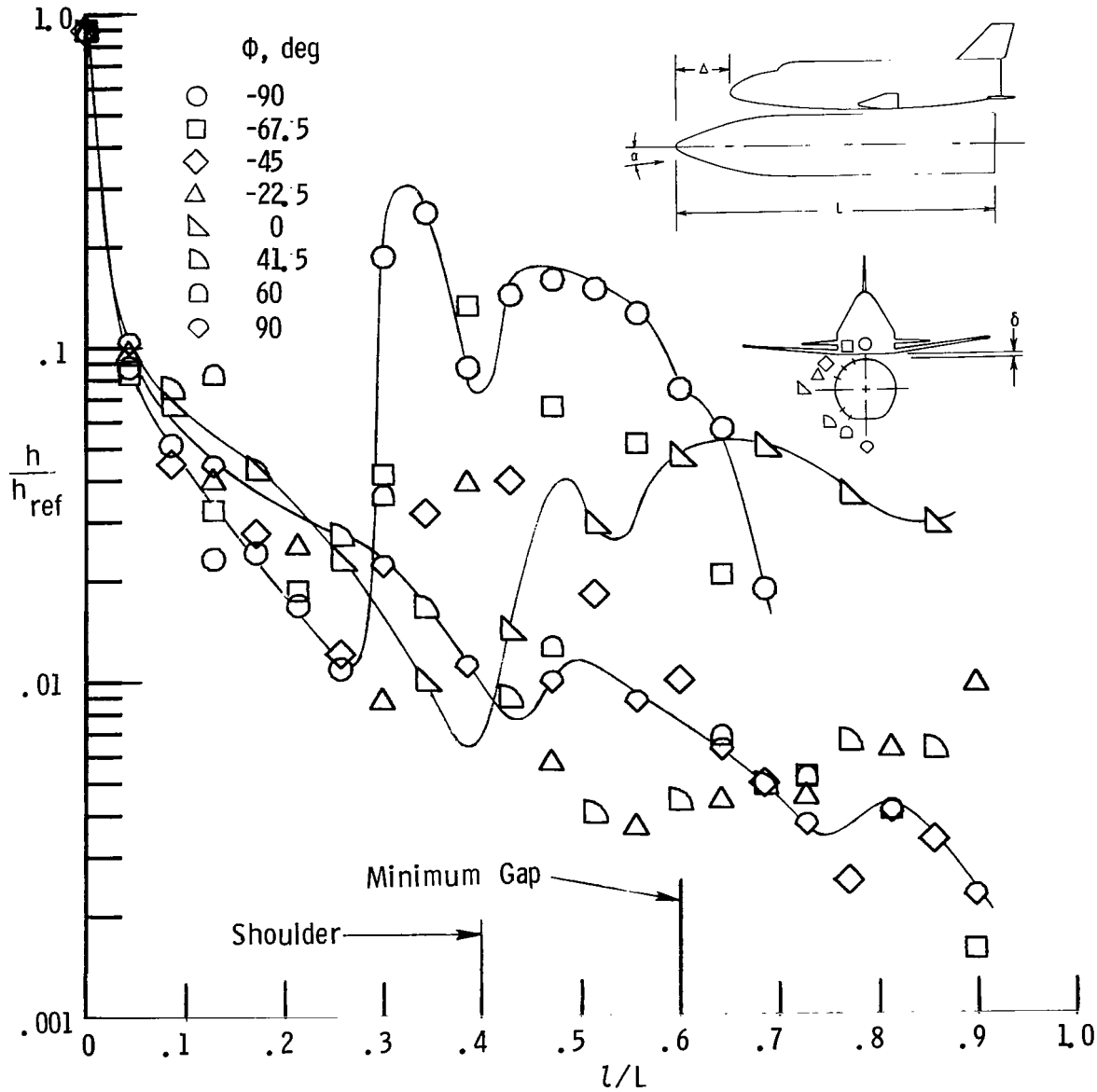

(e) $\alpha = 5^{o}$; $\delta/L = 0$; $\Delta/L = 0.17$.

Figure 6.- Continued.

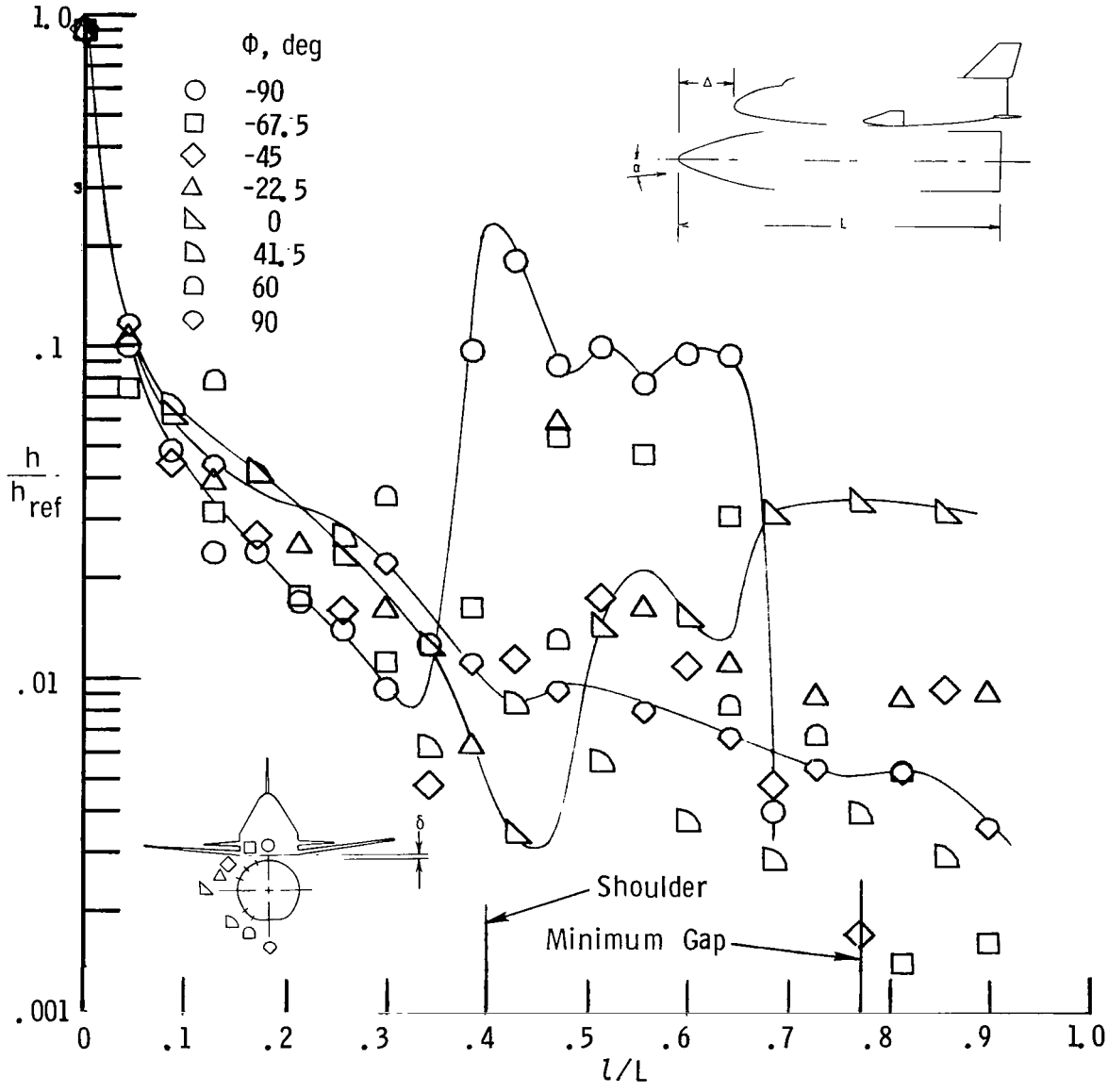

(f) $\alpha = 5^{o}$; $\delta/L = 0$; $\Delta/L = 0.34$.

Figure 6.- Continued.

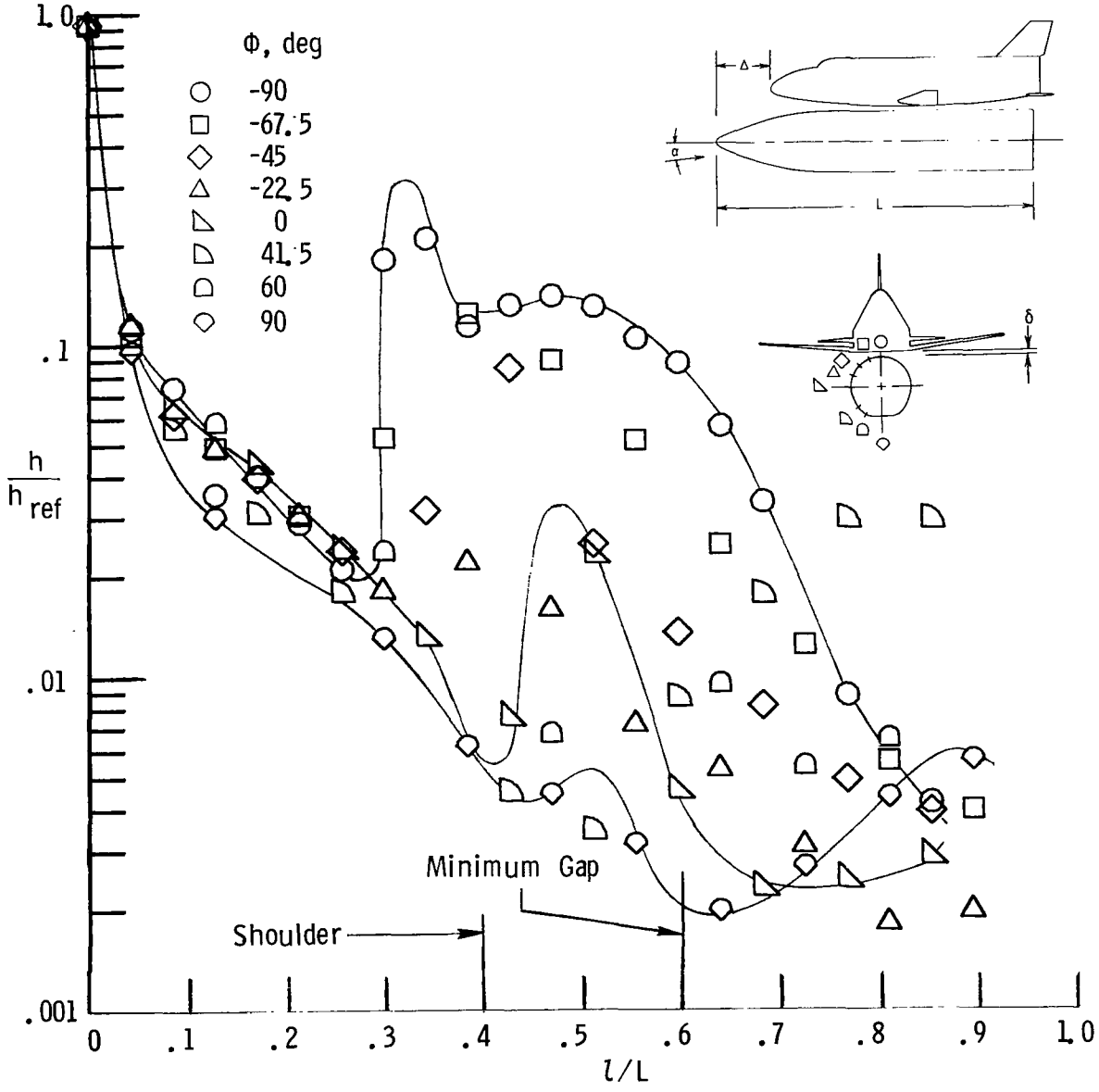

(g) $\alpha = 0^{o}$; $\delta/L = 0.0017$; $\Delta/L = 0.17$.

Figure 6.- Continued.

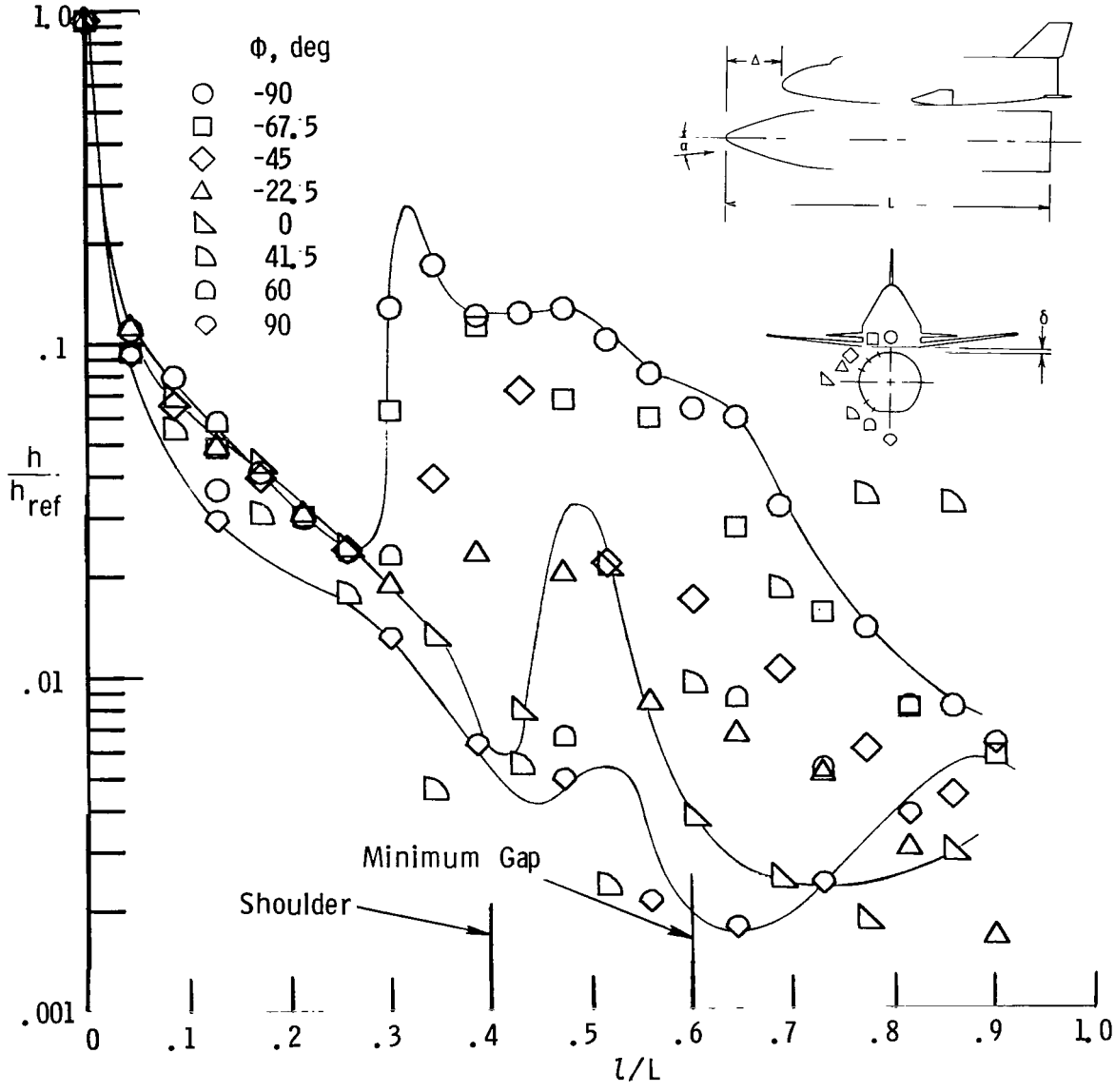

(h) $\alpha = 0^{o}$; $\delta/L = 0.0034$; $\Delta/L = 0.17$.

Figure 6.- Concluded.

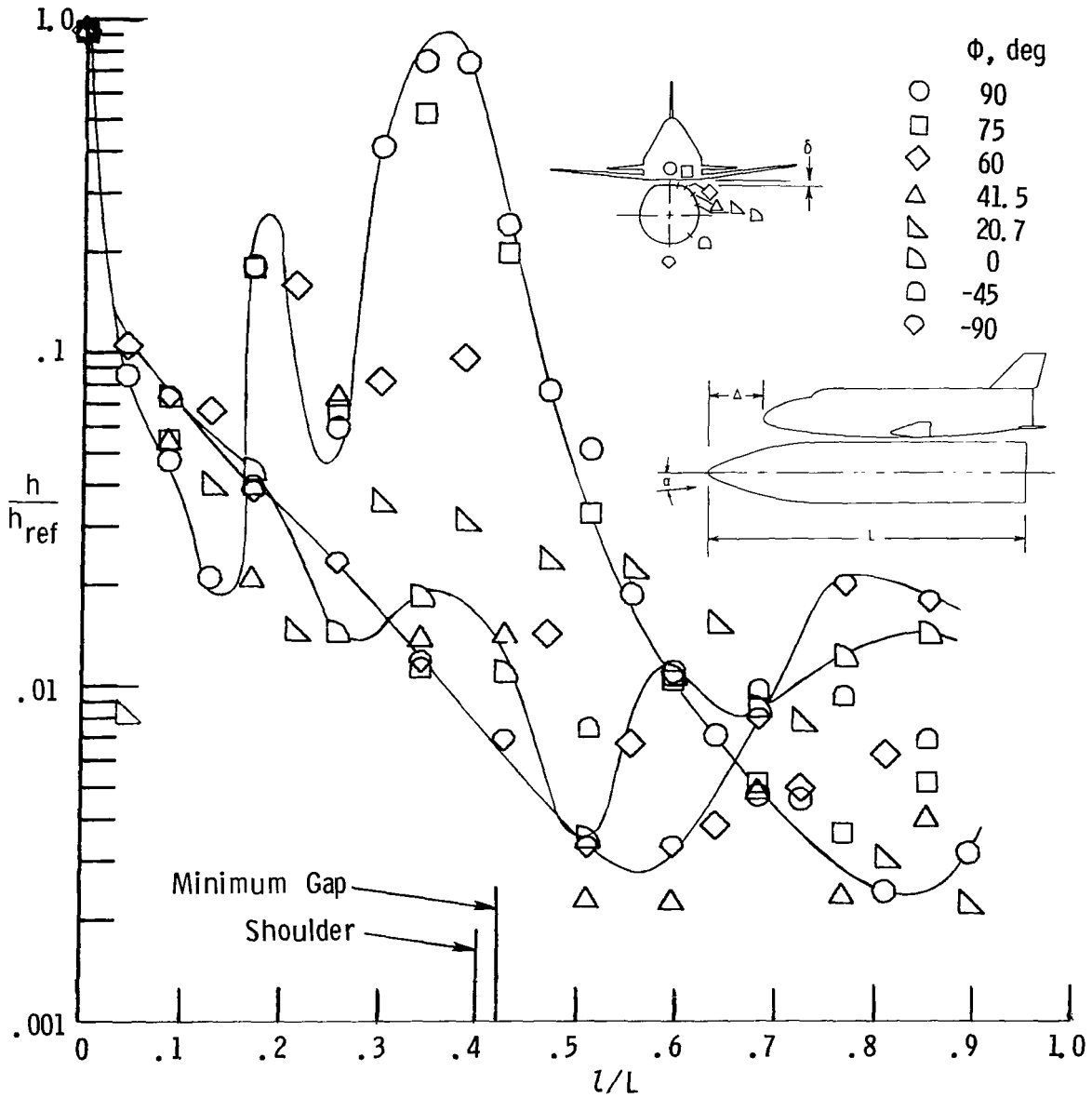

(a) $\alpha = 0^{o}$; $\delta/L = 0$; $\Delta/L = 0$.

Figure 7.- Heat transfer to tank with orbiter mated to flat side.

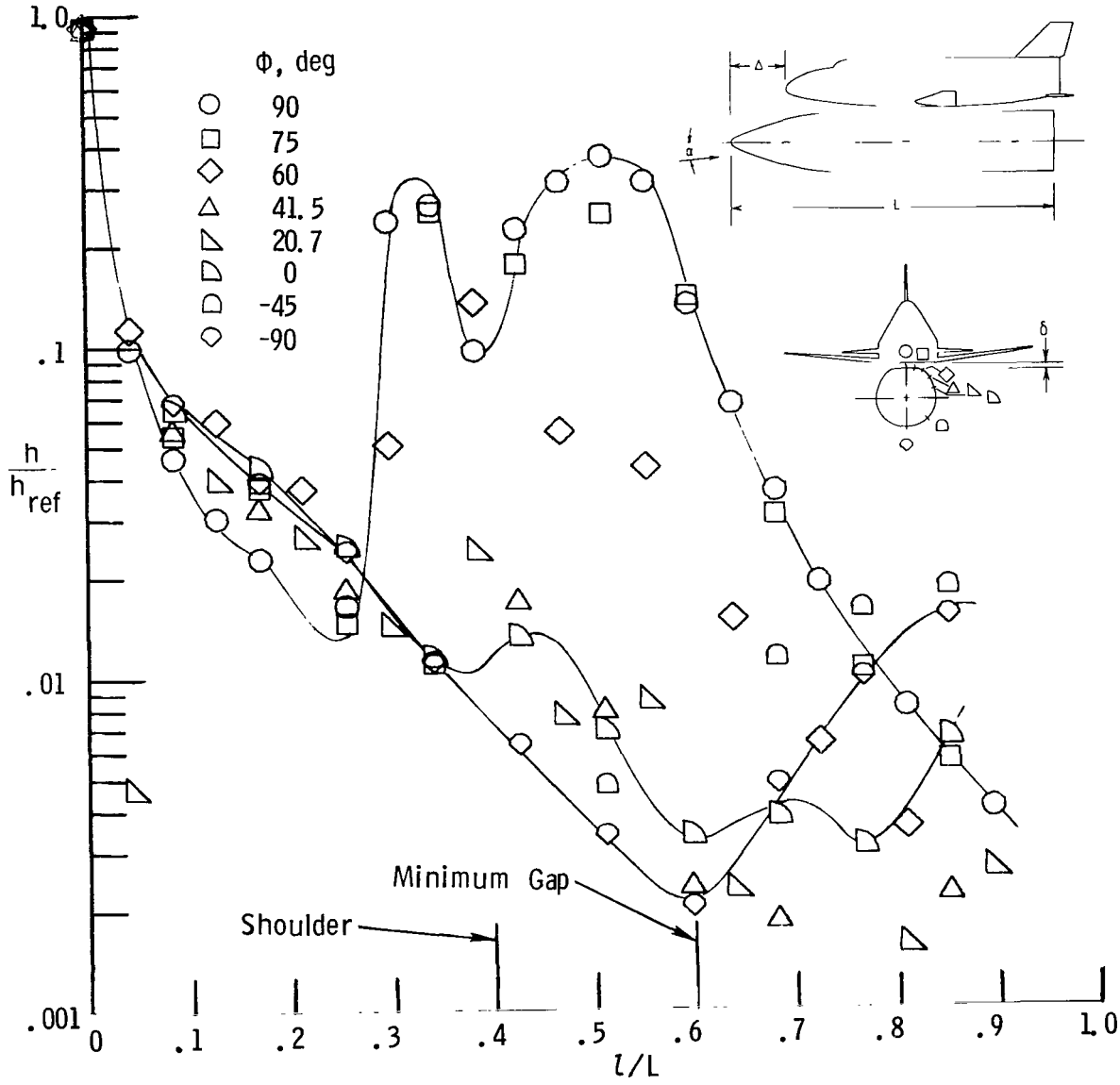

(b) $\alpha = 0^{o}$; $\delta/L = 0$; $\Delta/L = 0.17$.

Figure 7.- Continued.

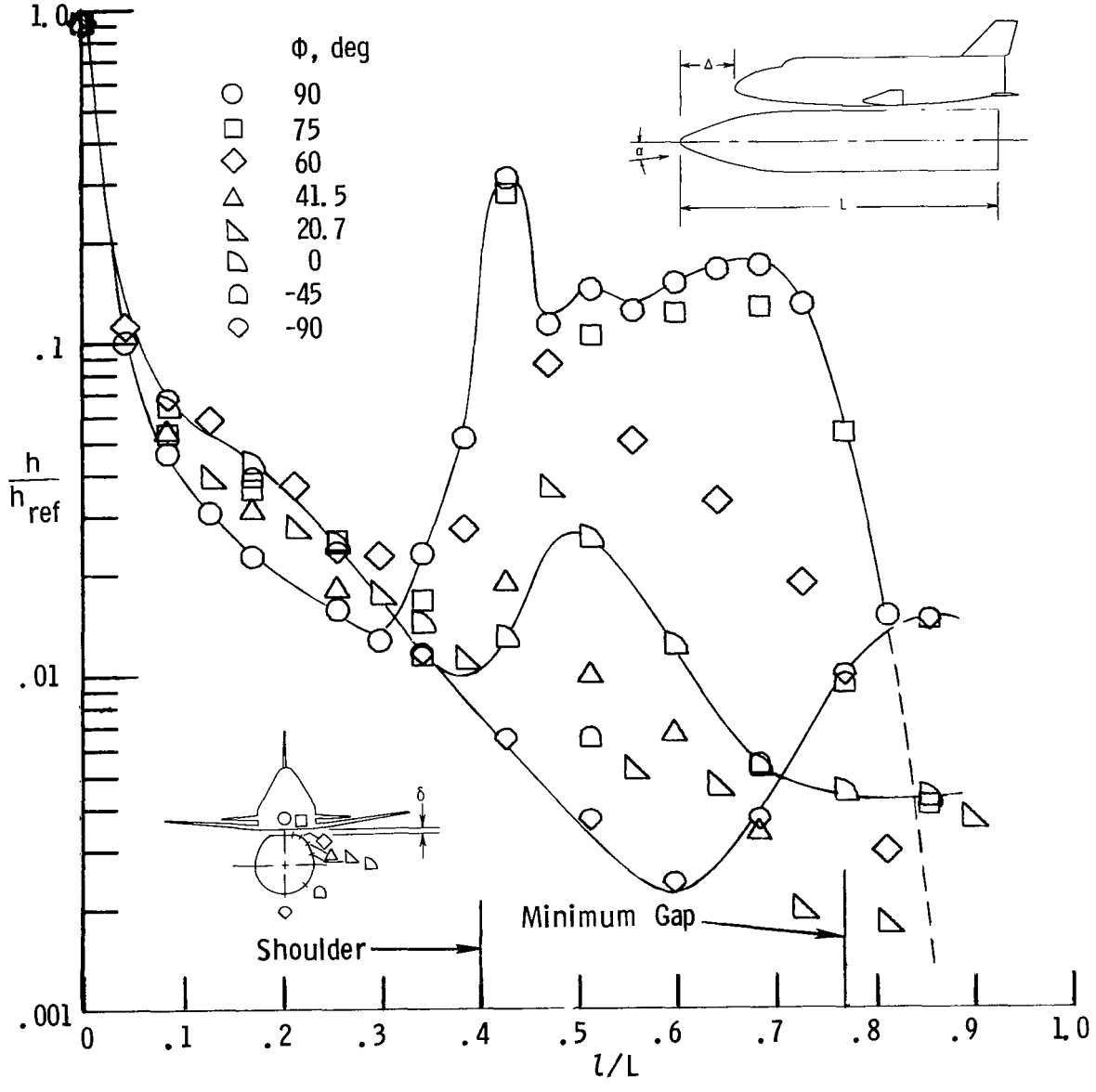

(c) $\alpha = 0^{o}$; $\delta/L = 0$; $\Delta/L = 0.34$.

Figure 7.- Continued.

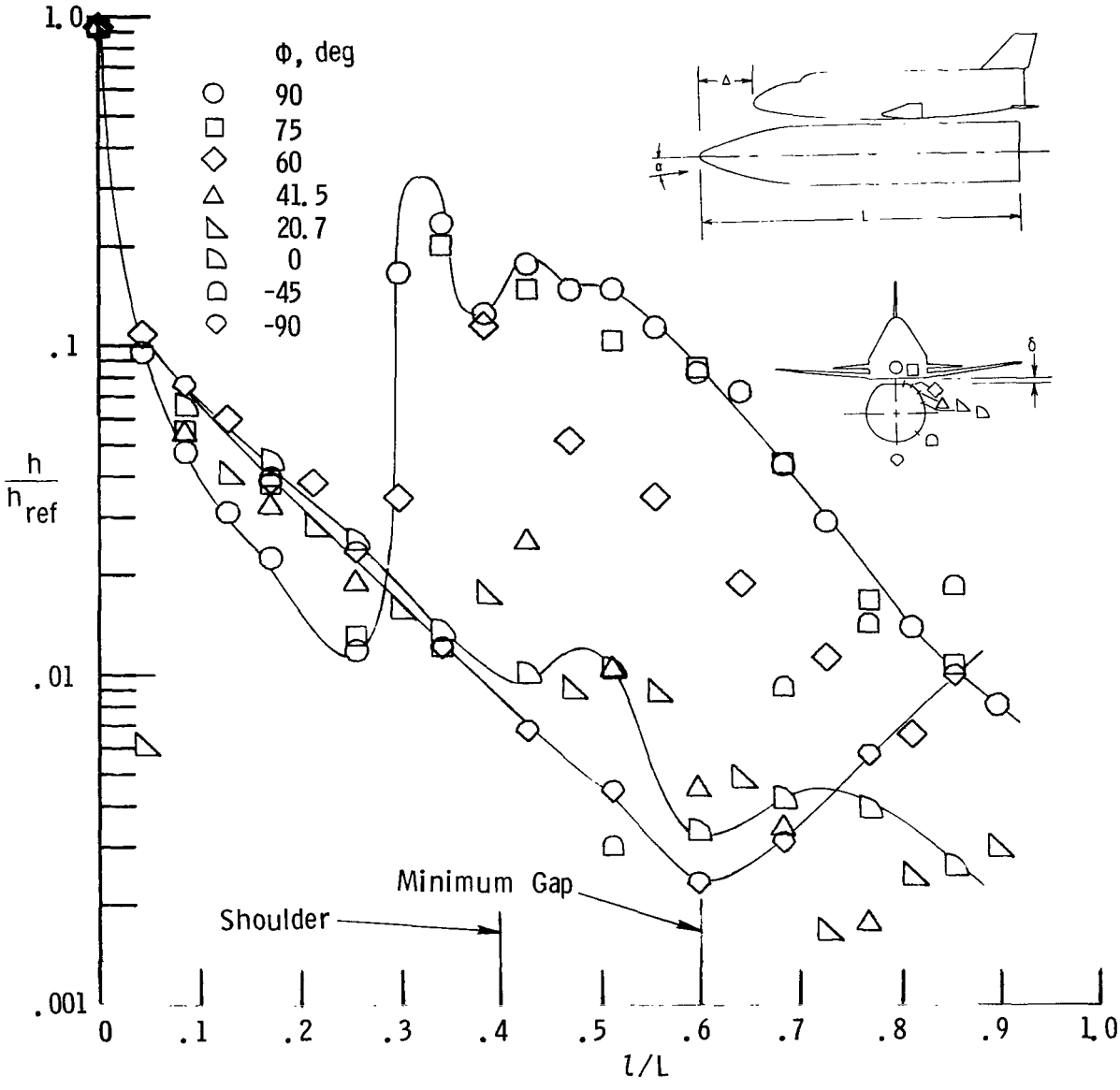

(d) $\alpha = 0^{o}$; $\delta/L = 0.0017$; $\Delta/L = 0.17$.

Figure 7.- Continued.

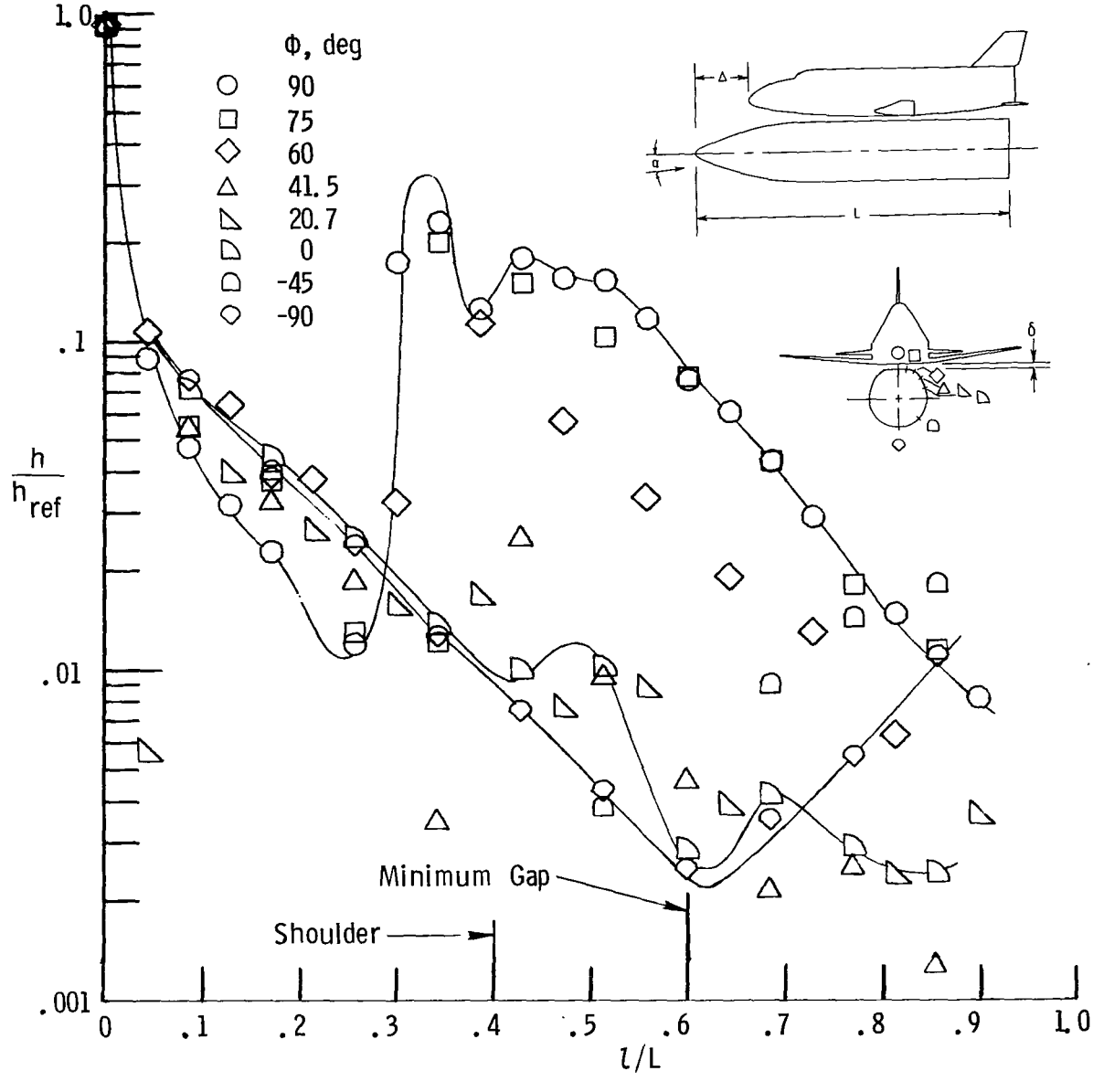

(e) $\alpha = 0^{o}$; $\delta/L = 0.0034$; $\Delta/L = 0.17$.

Figure 7.- Concluded.

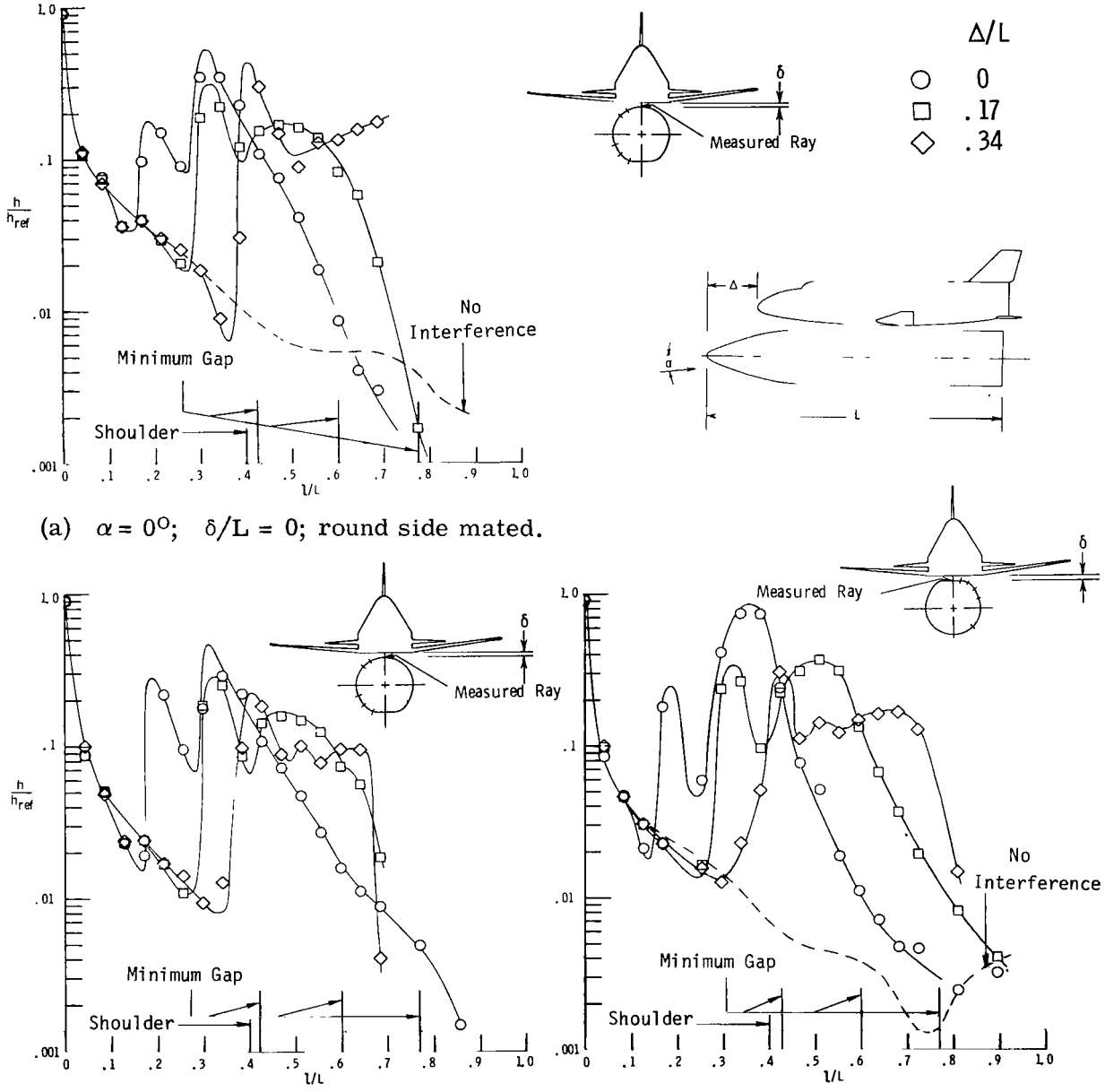

(a) $\alpha = 0^{o}$; $\delta/L = 0$; round side mated.

(b) $\alpha = 5^{o}$; $\delta/L = 0$; round side mated.

(c) $\alpha = 0^{o}$; $\delta/L = 0$; flat side mated.

Figure 8.- Heat transfer to adjacent ray of tank with orbiter mated to tank in three axial positions.

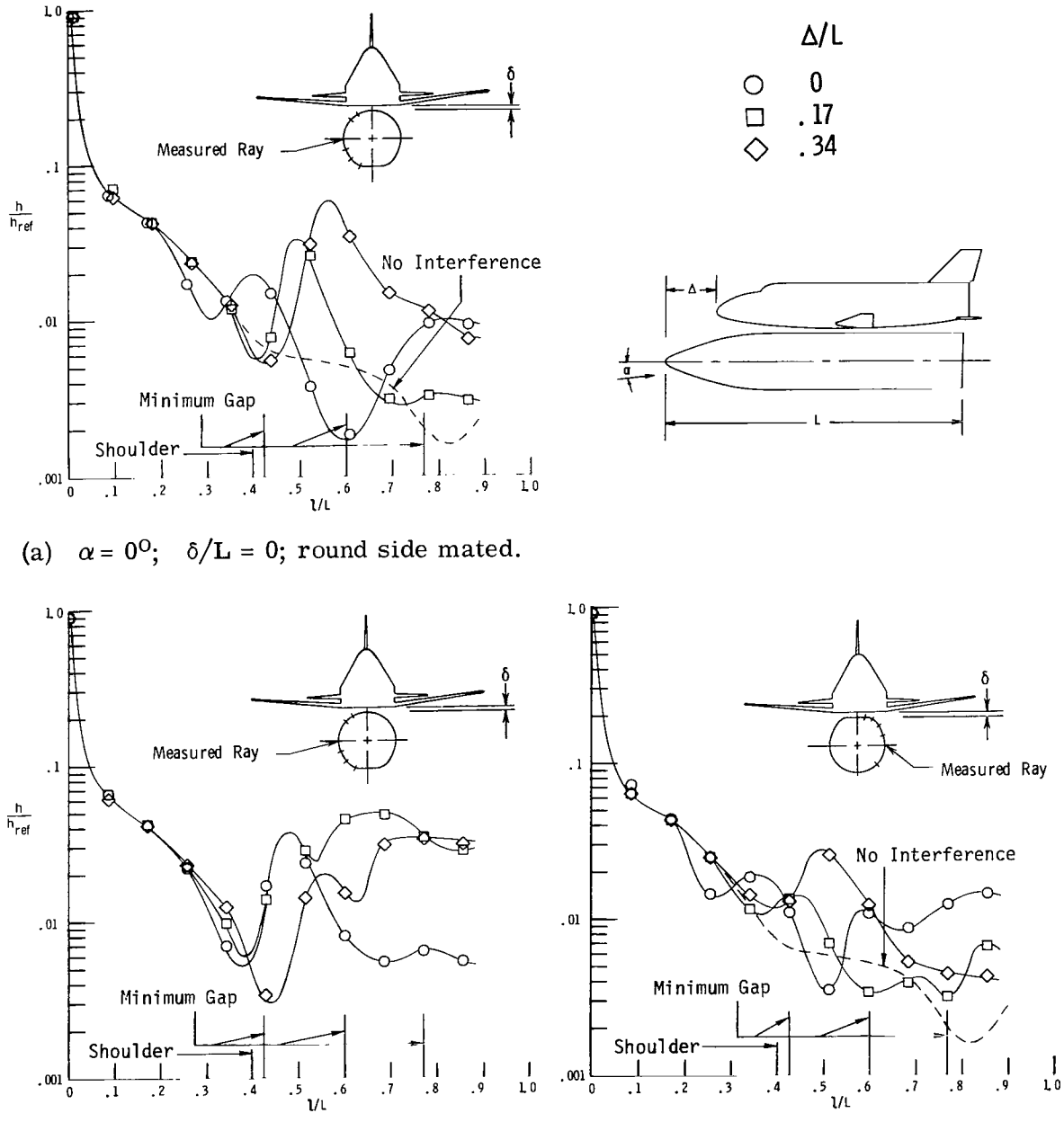

(a) $\alpha = 0^{o}$; $\delta/L = 0$; round side mated.

(b) $\alpha = 5^{o}$; $\delta/L = 0$; round side mated.

(c) $\alpha = 0^{o}$; $\delta/L = 0$; flat side mated.

Figure 9.- Heat transfer to side ray of tank with orbiter mated to tank in three axial positions.

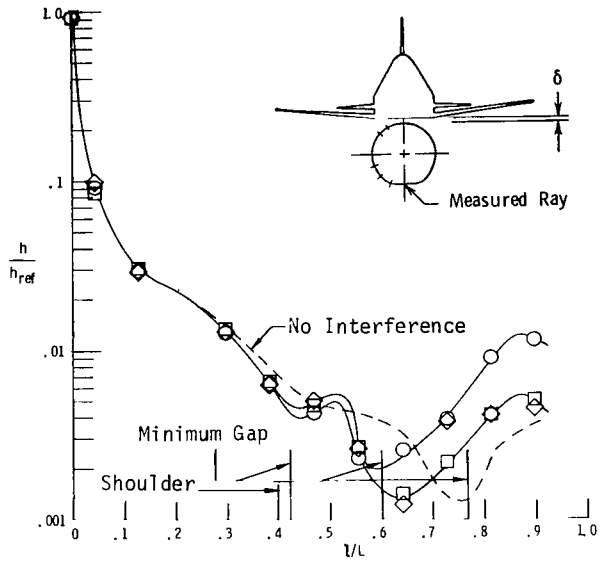

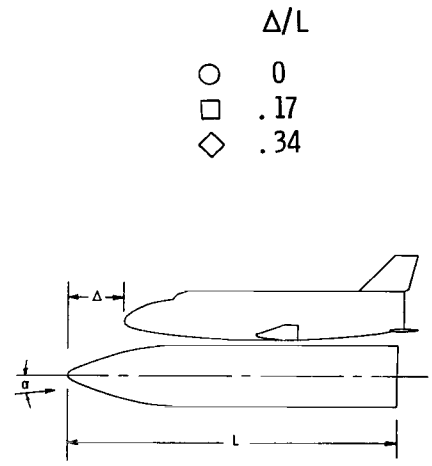

(a) $\alpha = 0^{o}$; $\delta/L = 0$; round side mated.

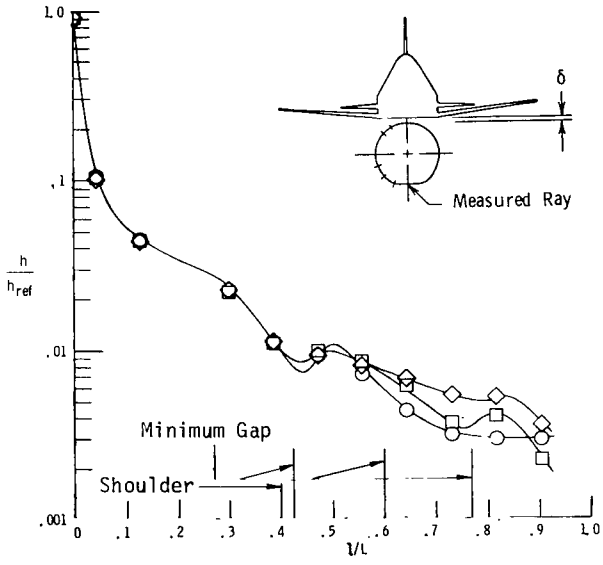

(b) $\alpha = 5^{o}$; $\delta/L = 0$; round side mated.

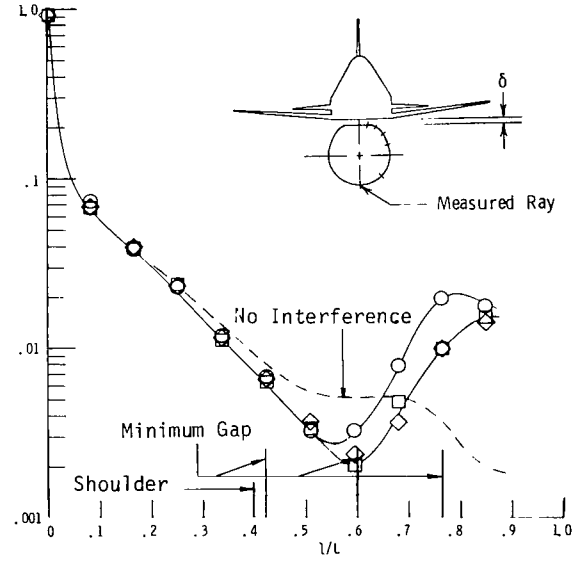

(c) $\alpha = 0^{o}$; $\delta/L = 0$; flat side mated.

Figure 10.- Heat transfer to opposite ray of tank with orbiter mated to tank in three axial positions.

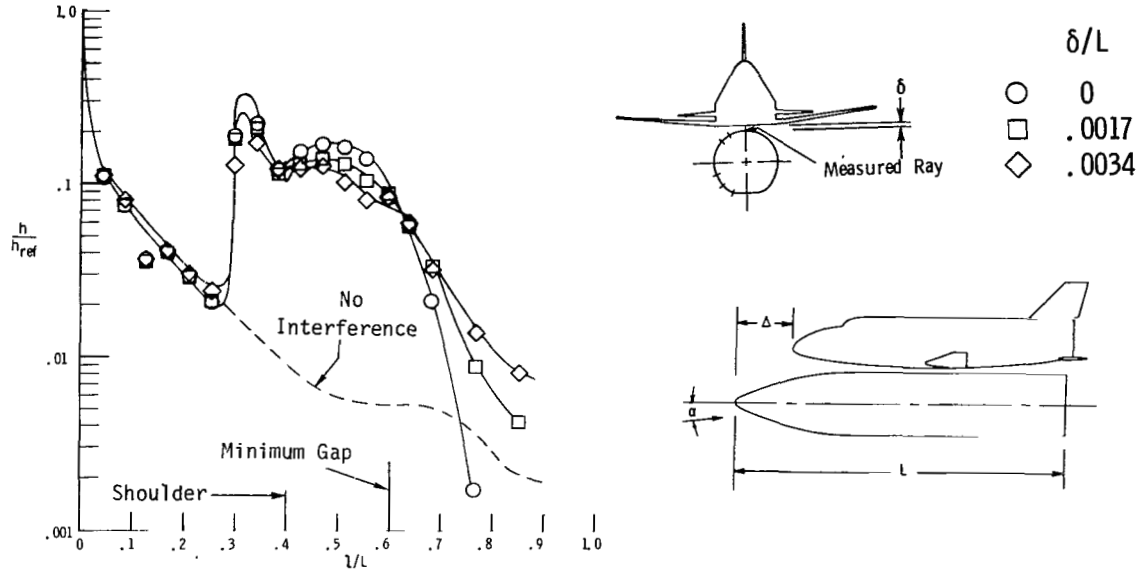

(a) $\alpha = 0^{o}$; $\Delta/L = 0.17$; adjacent ray.

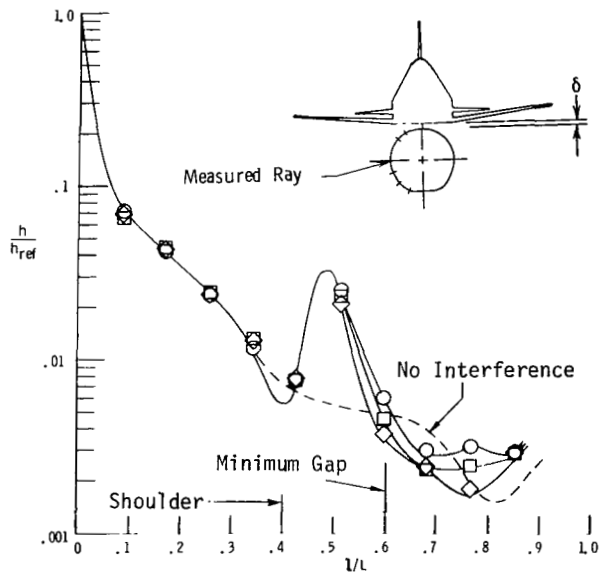

(b) $\alpha = 0^{o}$; $\Delta/L = 0.17$; side ray.

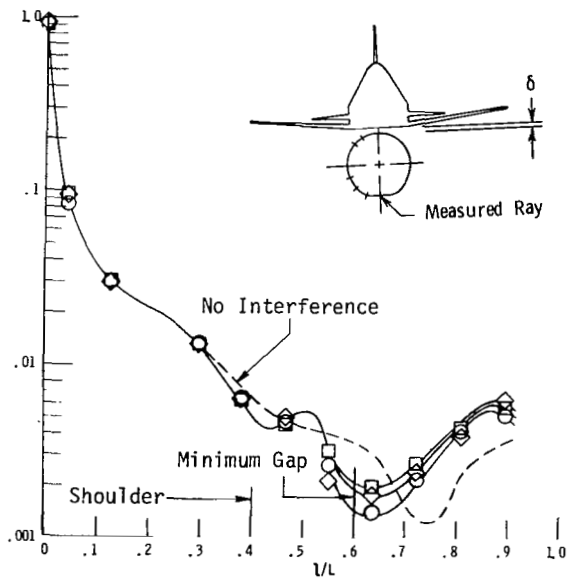

(c) $\alpha = 0^{o}$; $\Delta/L = 0.17$; opposite ray.

Figure 11.- Heat transfer to tank with orbiter mated to round side with three gap spacings from tank.

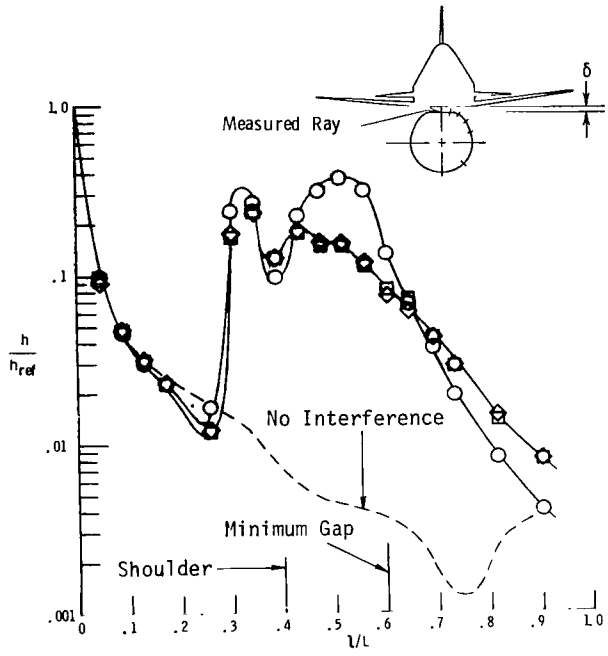

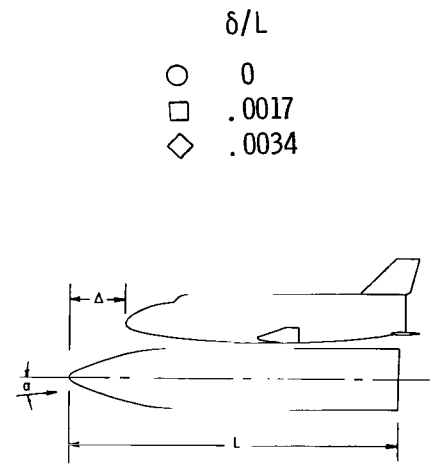

(a) $\alpha = 0^{o}$; $\Delta/L = 0.17$; adjacent ray.

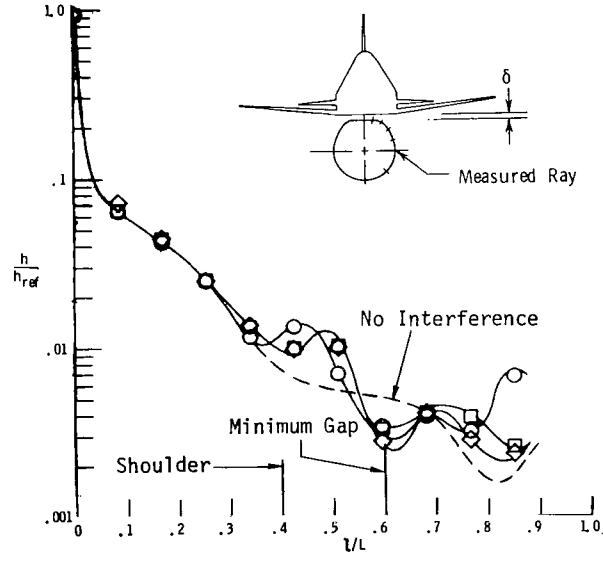

(b) $\alpha = 0^{o}$; $\Delta/L = 0.17$; side ray.

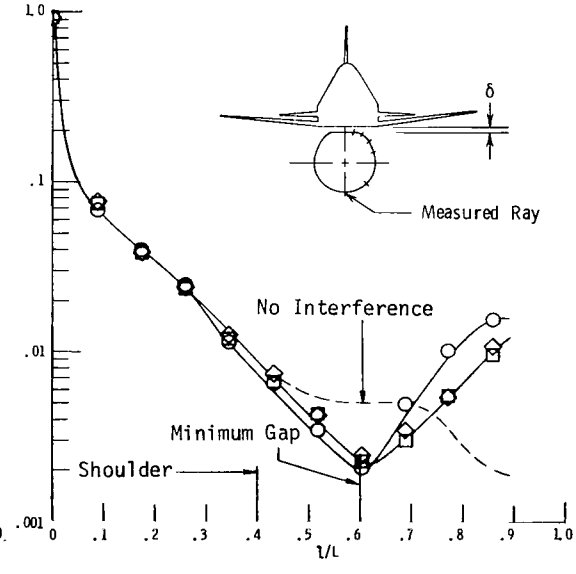

(c) $\alpha = 0^{o}$; $\Delta/L = 0.17$; opposite ray.

Figure 12.- Heat transfer to tank with orbiter mated to flat side with three gap spacings from tank.

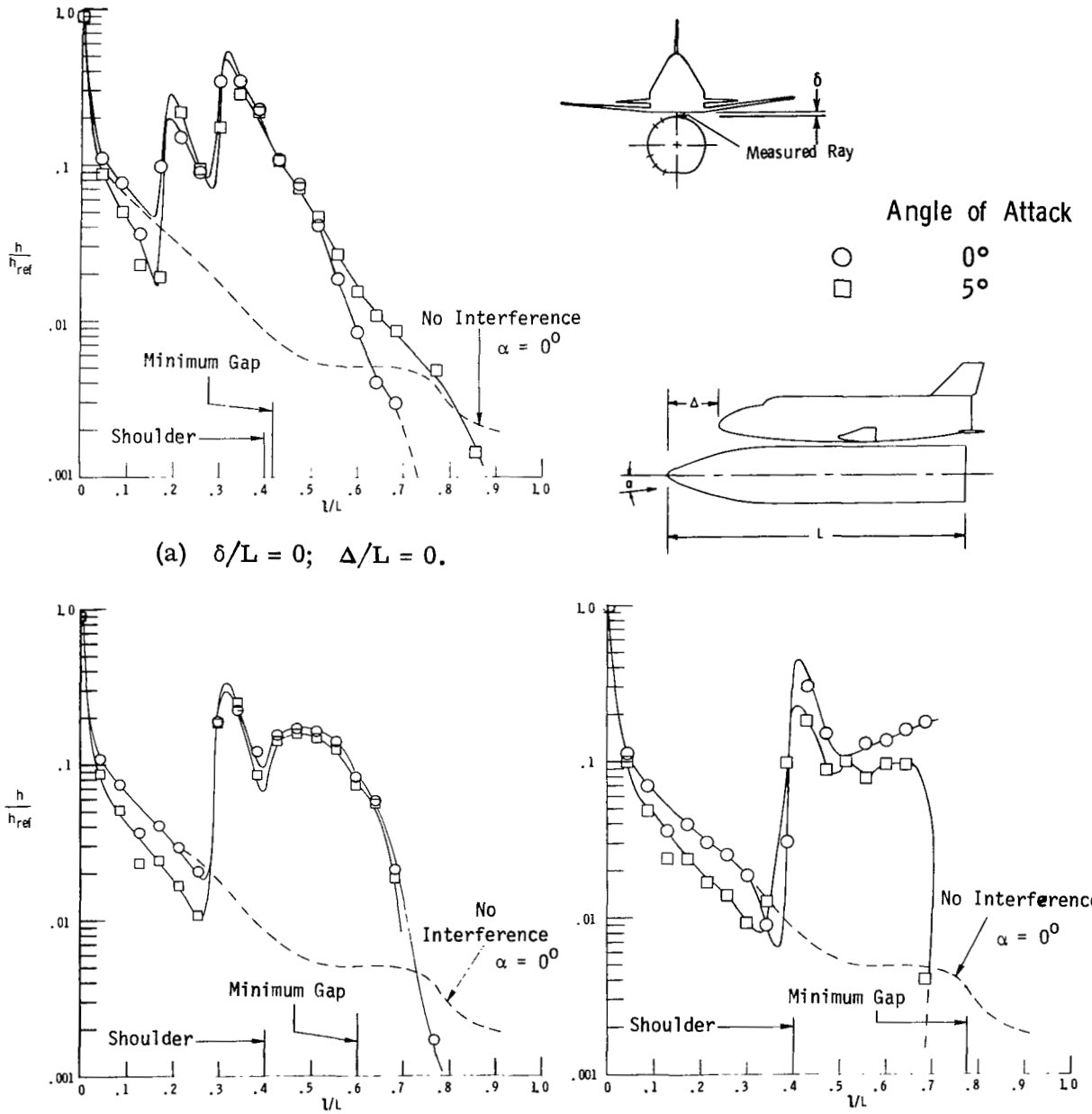

(a) $\delta/L = 0$; $\Delta/L = 0$.

(b) $\delta/L = 0$; $\Delta/L = 0.17$.

(c) $\delta/L = 0$; $\Delta/L = 0.34$.

Figure 13.- Comparison of heat transfer to adjacent ray of tank for orbiter-tank combination at two angles of attack with orbiter mated to round side.

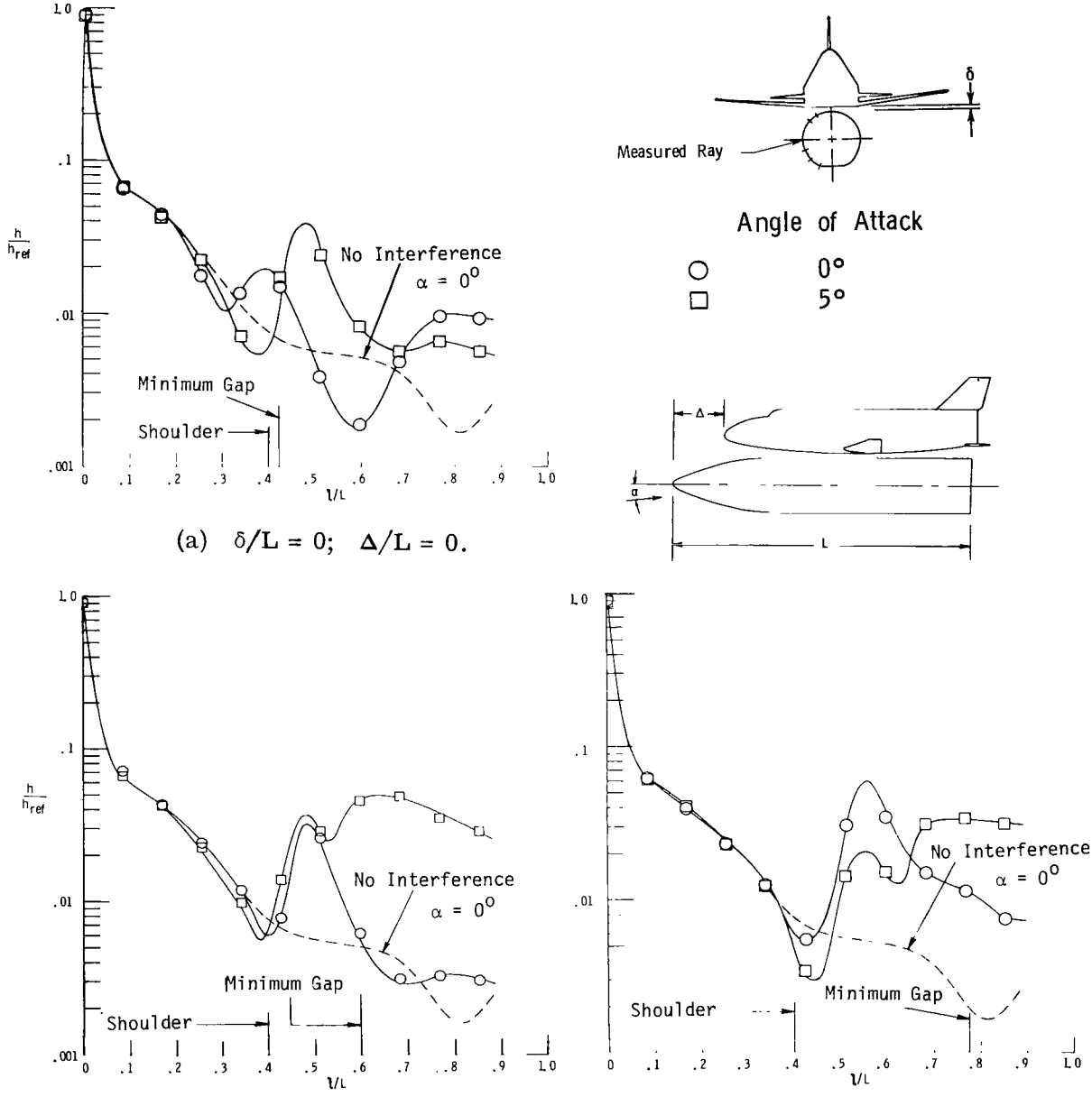

(a) $\delta/L = 0$; $\Delta/L = 0$.

(b) $\delta/L = 0$; $\Delta/L = 0.17$.

(c) $\delta/L = 0$; $\Delta/L = 0.34$.

Figure 14.- Comparison of heat transfer to side ray of tank for orbiter-tank combination at two angles of attack with orbiter mated to round side.

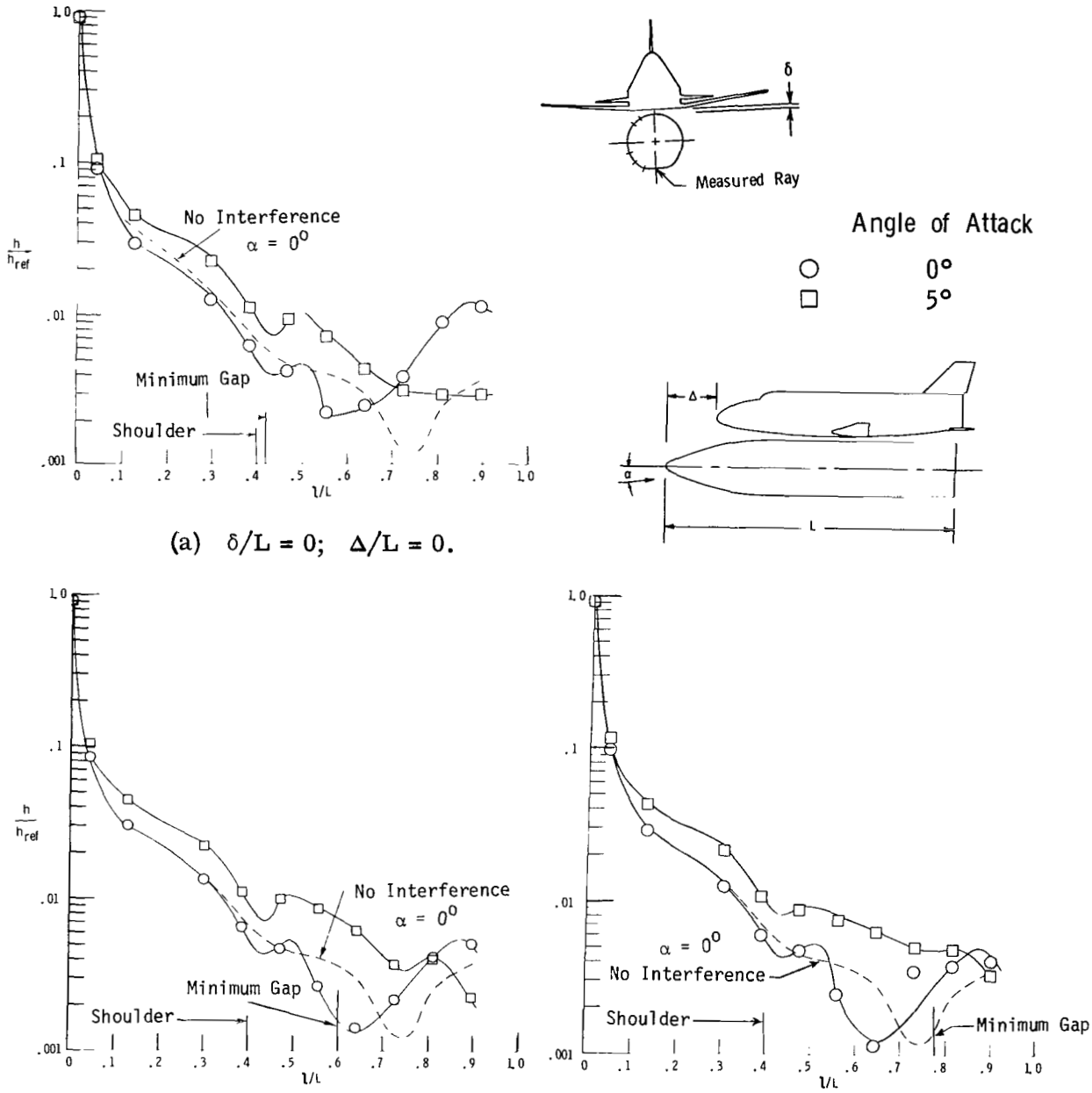

(a) $\delta/L = 0$; $\Delta/L = 0$.

(b) $\delta/L = 0$; $\Delta/L = 0.17$.

(c) $\delta/L = 0$; $\Delta/L = 0.34$.

Figure 15.- Comparison of heat transfer to opposite ray of tank for orbiter-tank combination at two angles of attack with orbiter.

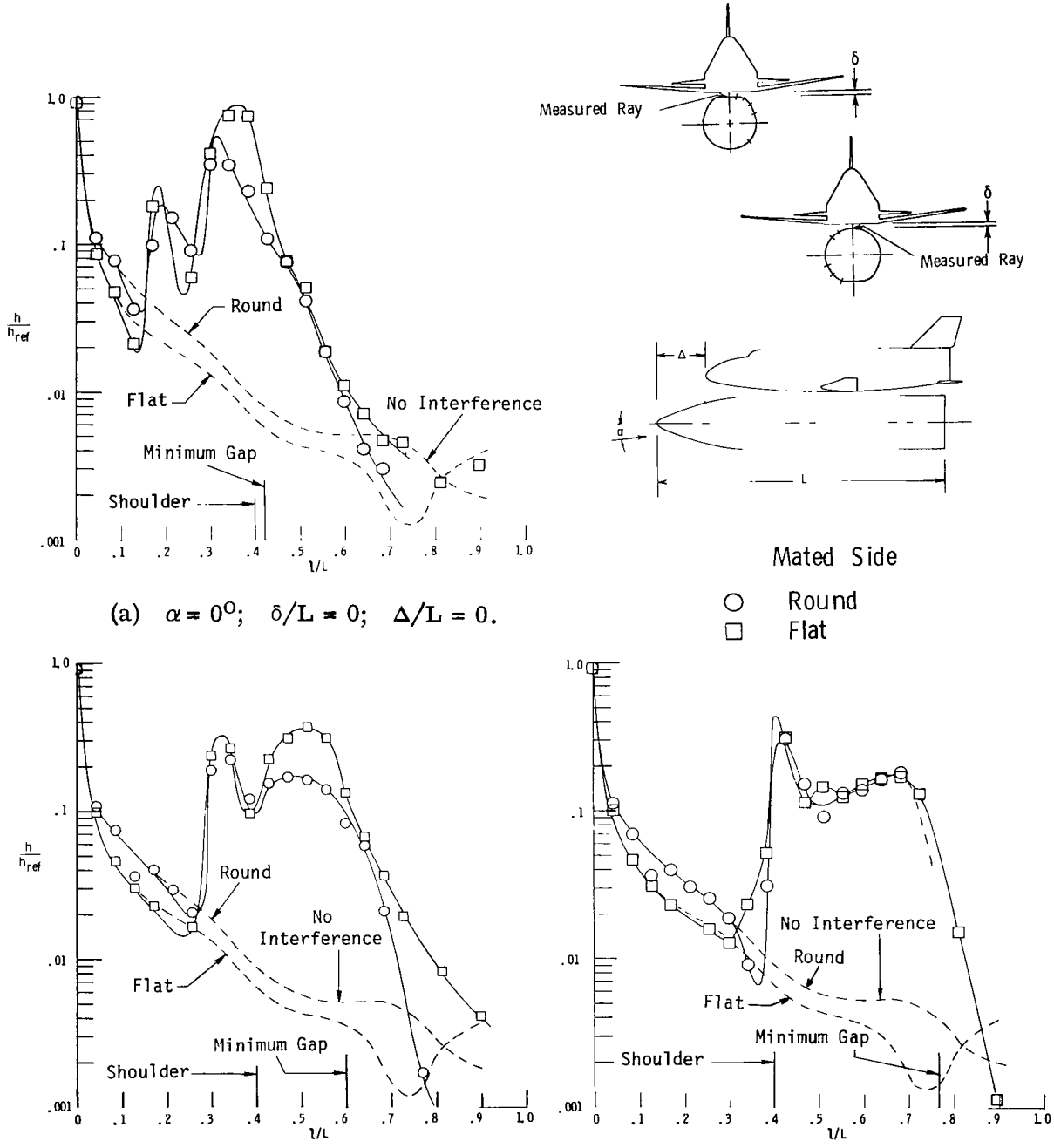

Figure 16.- Comparison of heat transfer to tank ray adjacent to orbiter mated to round side with that for orbiter mated to flat side for three axial positions.

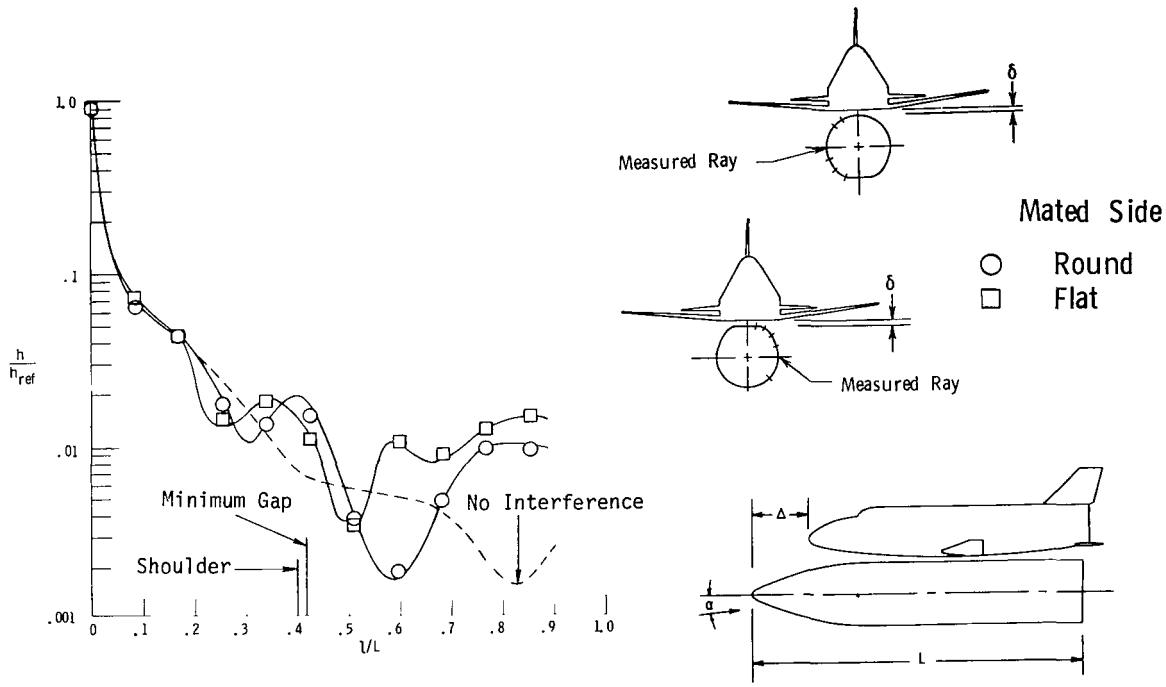

(a) $\alpha = 0^{o}$; $\delta/L = 0$; $\Delta/L = 0$.

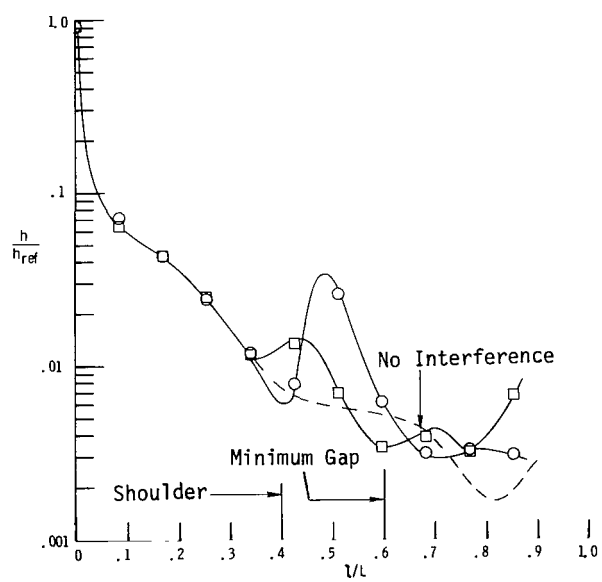

(b) $\alpha = 0^{o}$; $\delta/L = 0$; $\Delta/L = 0.17$.

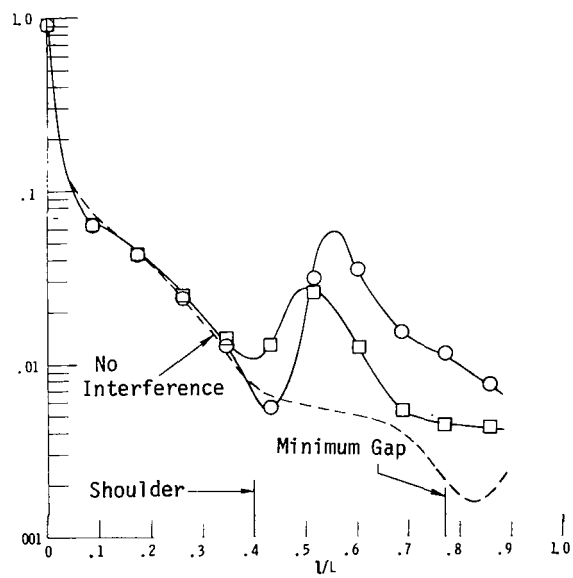

(c) $\alpha = 0^{o}$; $\delta/L = 0$; $\Delta/L = 0.34$.

Figure 17.- Comparison of heat transfer to tank side ray with orbiter mated to round side with that to tank side ray with orbiter mated to flat side for three axial positions.

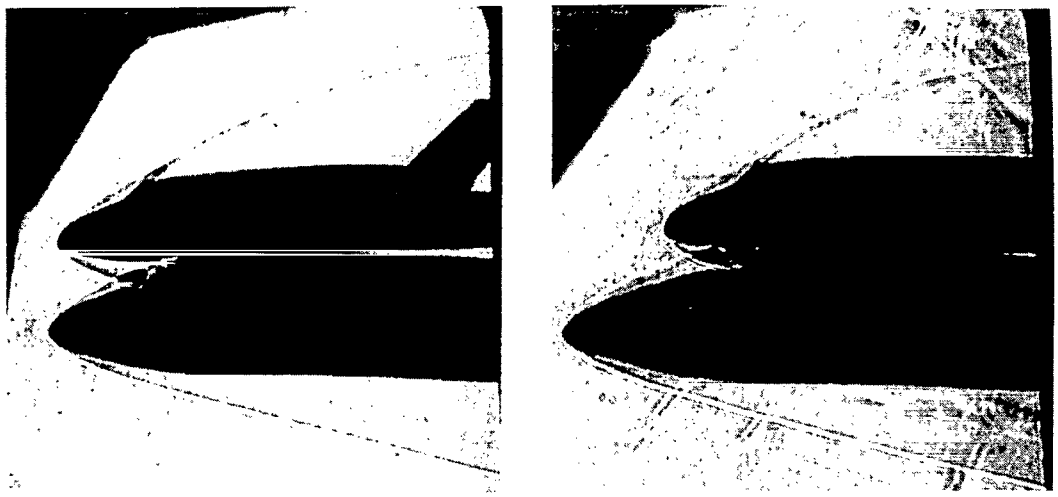

Δ/L = 0; α = 0°; Gap = 0

Δ/L = 0.17; α = 0°; Gap = 0.0034

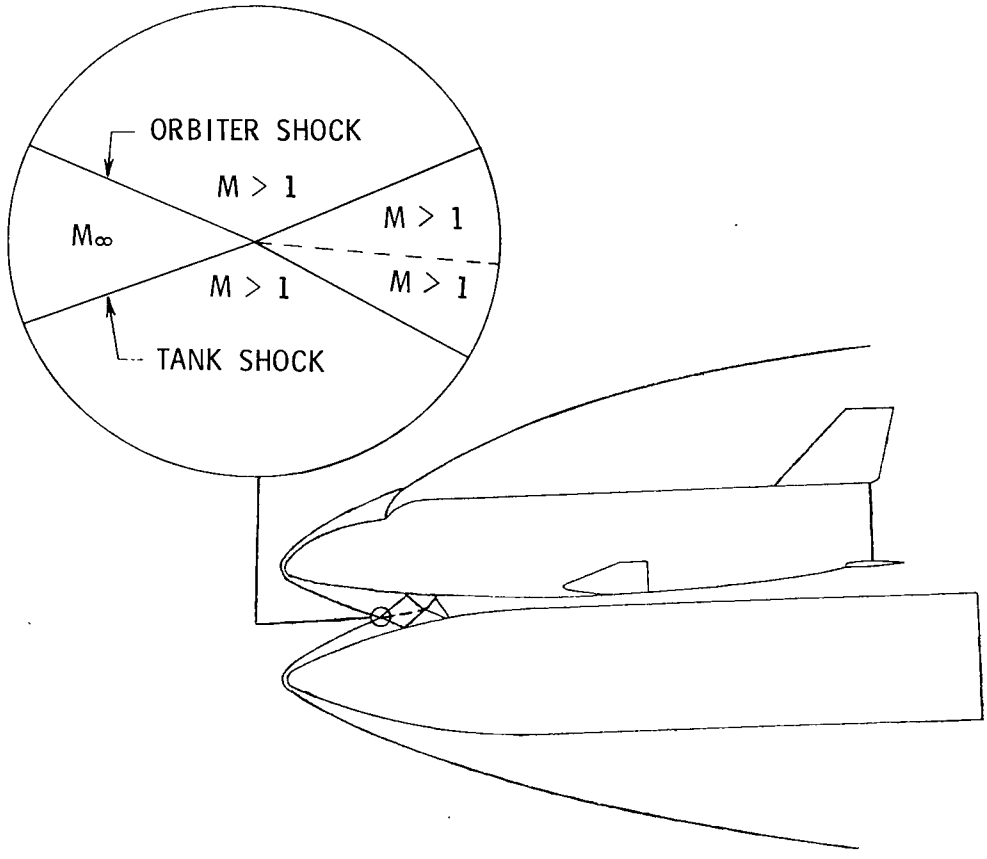

L-76-144

Figure 18.- Examples of Edney type I shock intersection pattern.

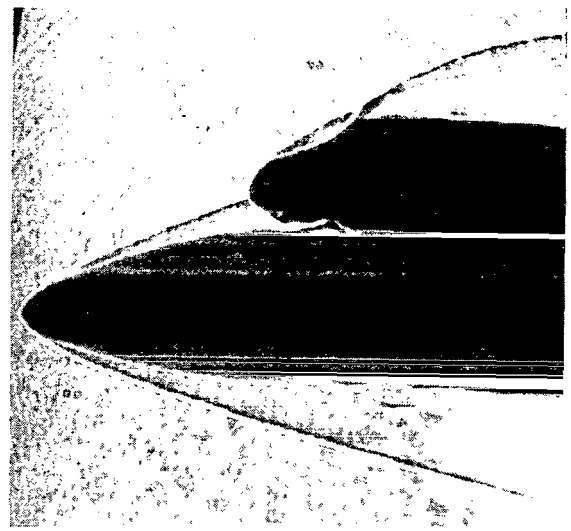

$\Delta/L = 0.34; \alpha = 0°;$ Gap = 0

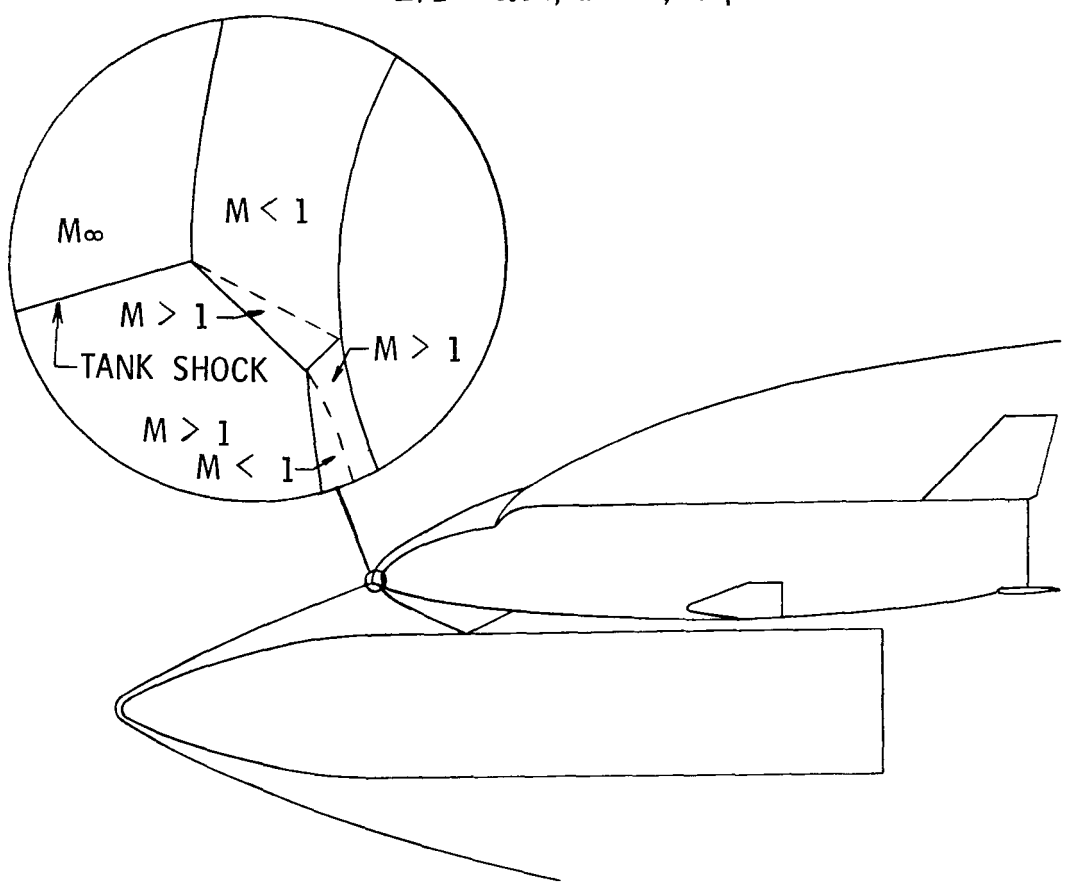

L-76-145

Figure 19.- Example of possible Edney type III intersection pattern.

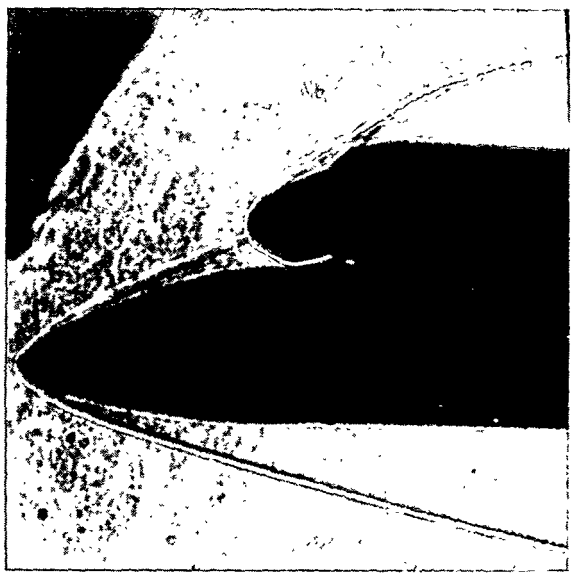

$\Delta/L = 0.34; \alpha = 0°; \text{Gap} = 0$

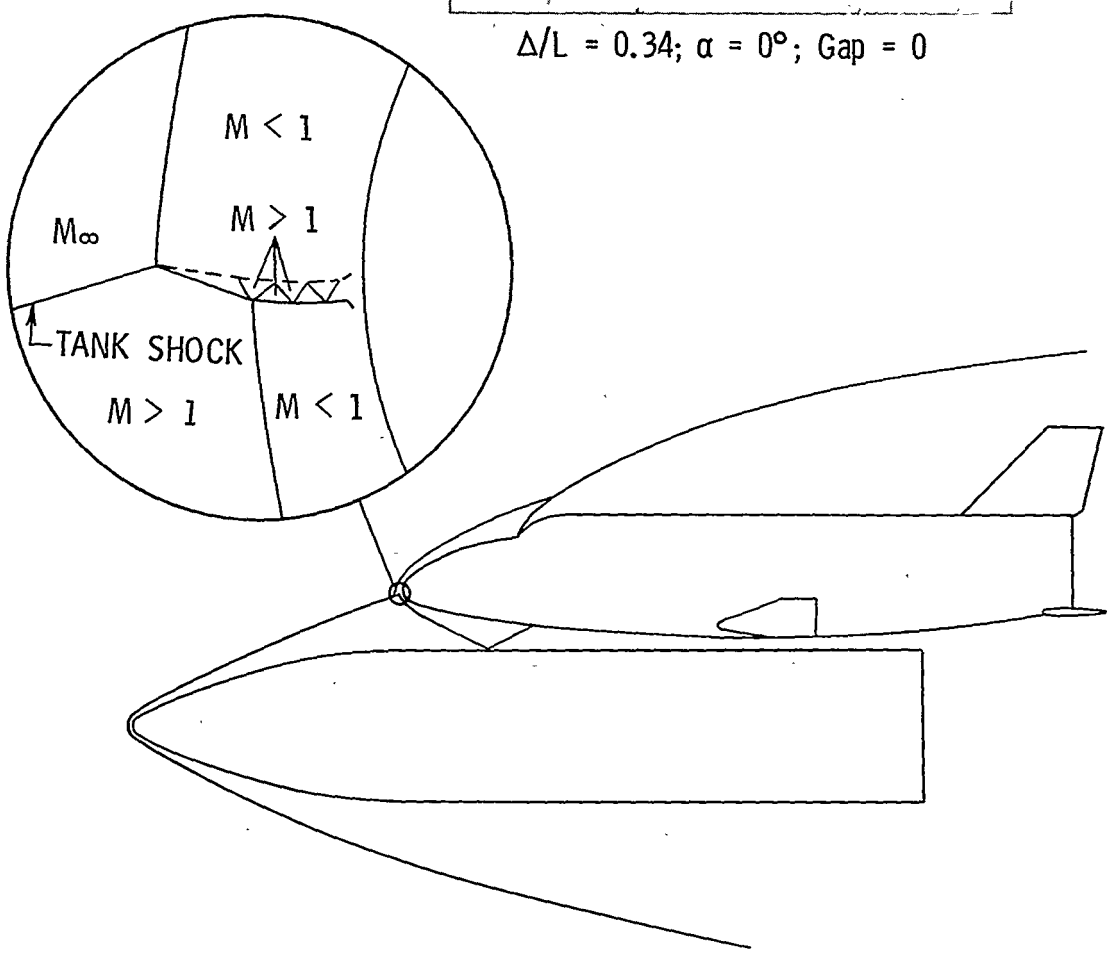

L-76-146

Figure 20.- Example of possible Edney type IV shock intersection pattern.

$\Delta/L = 0.34$; $\alpha = 5°$; Gap = 0

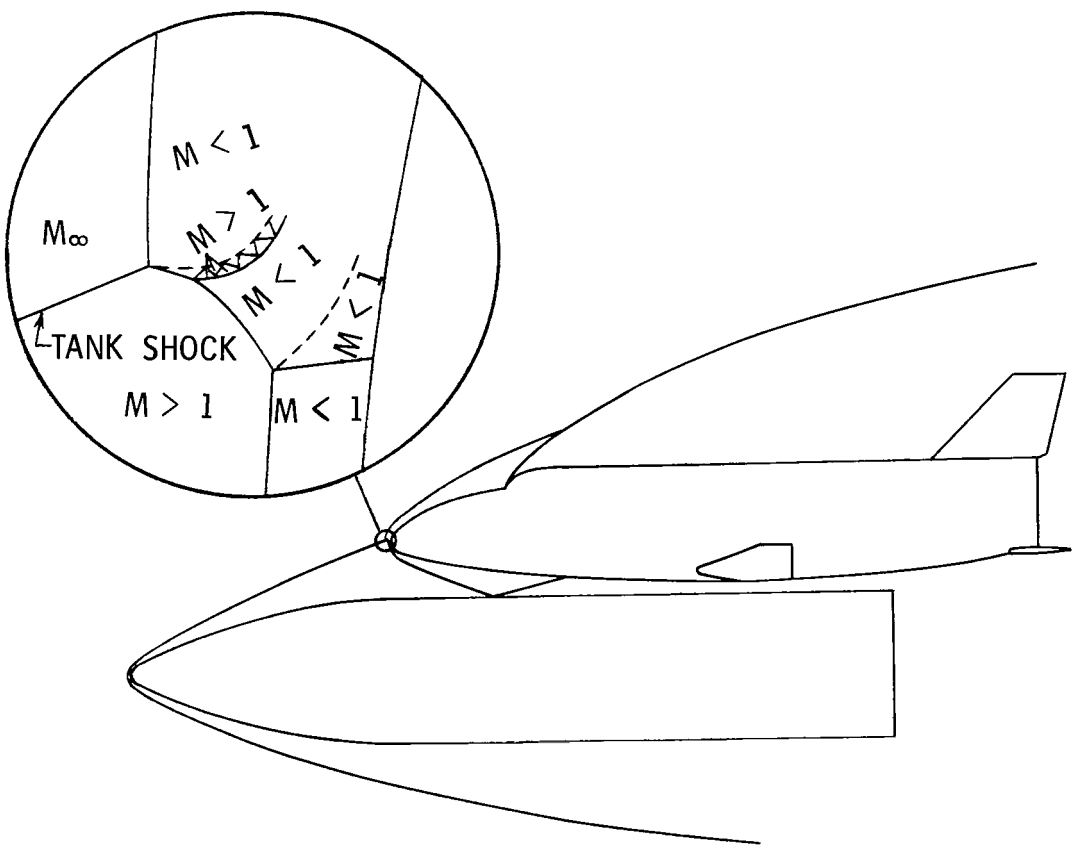

L-76-147

Figure 21.- Example of possible Edney type V shock intersection pattern.

"The aeronautical and space activities of the United States shall be conducted so as to contribute . . . to the expansion of human knowledge of phenomena in the atmosphere and space. The Administration shall provide for the widest practicable and appropriate dissemination of information concerning its activities and the results thereof."

—NATIONAL AERONAUTICS AND SPACE ACT OF 1958

NASA SCIENTIFIC AND TECHNICAL PUBLICATIONS

TECHNICAL REPORTS: Scientific and technical information considered important, complete, and a lasting contribution to existing knowledge.

TECHNICAL NOTES: Information less broad in scope but nevertheless of importance as a contribution to existing knowledge.

TECHNICAL MEMORANDUMS: Information receiving limited distribution because of preliminary data, security classification, or other reasons. Also includes conference proceedings with either limited or unlimited distribution.

CONTRACTOR REPORTS: Scientific and technical information generated under a NASA contract or grant and considered an important contribution to existing knowledge.

TECHNICAL TRANSLATIONS: Information published in a foreign language considered to merit NASA distribution in English.

SPECIAL PUBLICATIONS: Information derived from or of value to NASA activities. Publications include final reports of major projects, monographs, data compilations, handbooks, sourcebooks, and special bibliographies.

TECHNOLOGY UTILIZATION PUBLICATIONS: Information on technology used by NASA that may be of particular interest in commercial and other non-aerospace applications. Publications include Tech Briefs, Technology Utilization Reports and Technology Surveys.

Details on the availability of these publications may be obtained from:

SCIENTIFIC AND TECHNICAL INFORMATION OFFICE

NATIONAL AERONAUTICS AND SPACE ADMINISTRATION

Washington, D.C. 20546